



## Iron isotope fractionation in subterranean estuaries

Olivier Rouxel<sup>a,\*</sup>, Edward Sholkovitz<sup>a</sup>, Matthew Charette<sup>a</sup>, Katrina J. Edwards<sup>a,b</sup>

<sup>a</sup> Woods Hole Oceanographic Institution, Marine Chemistry and Geochemistry Department, MS#25, Woods Hole, MA 02543, USA

<sup>b</sup> Department of Biological Sciences, University of Southern California, Los Angeles, CA 90089-0371, USA

Received 25 April 2007; accepted in revised form 1 May 2008

### Abstract

Dissolved Fe concentrations in subterranean estuaries, like their river-seawater counterparts, are strongly controlled by non-conservative behavior during mixing of groundwater and seawater in coastal aquifers. Previous studies at a subterranean estuary of Waquoit Bay on Cape Cod, USA demonstrate extensive precipitation of groundwater-borne dissolved ferrous iron and subsequent accumulation of iron oxides onto subsurface sands. Waquoit Bay is thus an excellent natural laboratory to assess the mechanisms of Fe-isotope fractionation in redox-stratified environments and determine potential Fe-isotope signatures of groundwater sources to coastal seawater. Here, we report Fe isotope compositions of iron-coated sands and porewaters beneath the intertidal zone of Waquoit Bay. The distribution of pore water Fe shows two distinct sources of Fe: one residing in the upward rising plume of Fe-rich groundwater and the second in the salt-wedge zone of pore water. The groundwater source has high Fe(II) concentration consistent with anoxic conditions and yield  $\delta^{56}\text{Fe}$  values between 0.3 and  $-1.3\text{‰}$ . In contrast, sediment porewaters occurring in the mixing zone of the subterranean estuary have very low  $\delta^{56}\text{Fe}$  values down to  $-5\text{‰}$ . These low  $\delta^{56}\text{Fe}$  values reflect Fe-redox cycling and result from the preferential retention of heavy Fe-isotopes onto newly formed Fe-oxyhydroxides. Analysis of Fe-oxides precipitated onto subsurface sands in two cores from the subterranean estuary revealed strong  $\delta^{56}\text{Fe}$  and Fe concentration gradients over less than 2m, yielding an overall range of  $\delta^{56}\text{Fe}$  values between  $-2$  and  $1.5\text{‰}$ . The relationship between Fe concentration and  $\delta^{56}\text{Fe}$  of Fe-rich sands can be modeled by the progressive precipitation of Fe-oxides along fluid flow through the subterranean estuary. These results demonstrate that large-scale Fe isotope fractionation (up to  $5\text{‰}$ ) can occur in subterranean estuaries, which could lead to coastal seawater characterized by very low  $\delta^{56}\text{Fe}$  values relative to river values.

© 2008 Published by Elsevier Ltd.

### 1. INTRODUCTION

Iron is a particle reactive trace metal present at extremely low concentrations in the upper ocean ( $<1$  nM) (e.g. Wu et al., 2001; Boyle et al., 2005) and is now recognized as a limiting nutrient in large regions of world's ocean and in certain coastal waters (Martin, 1990; Hutchins et al., 1999; Archer and Johnson, 2000; Boyd et al., 2000). The main sources of dissolved Fe into the ocean are atmospheric deposition, input from rivers, re-suspended sediment and pore water along continental shelves and hydrothermal vents (e.g. Wells et al., 1995; Elderfield and

Schultz, 1996; Johnson et al., 1999). In contrast to the interior of the oceans, marine sediments and rivers are important sources of iron to the water column of coastal systems (e.g., Hutchins et al., 1999; Johnson et al., 1999; Elrod et al., 2004; Mayer, 1982; Powell and Wilson-Finelli, 2003; Jickells et al., 2005; Buck et al., 2007; Ussher et al., 2007).

The stable isotope composition of Fe can provide valuable insights into the sources of Fe and Fe biogeochemical cycles in marine and terrestrial environment. In particular, significant fractionation of Fe isotopes has been demonstrated during partial oxidation and reduction reactions, suggesting that Fe isotopes are useful tracers of Fe redox cycling (Beard et al., 2003b; Johnson et al., 2004; Rouxel et al., 2005; Staubwasser et al., 2005; Teutsch et al., 2005; Severmann et al., 2006; Anbar and Rouxel, 2007; de Jong

\* Corresponding author. Fax: +1 508 457 2013.  
E-mail address: orouxel@whoi.edu (O. Rouxel).

et al., 2007). These redox processes include dissimilatory Fe(III) reduction (Beard et al., 1999; Beard et al., 2003a; Crosby et al., 2007; Icopini et al., 2004), anaerobic photosynthetic Fe(II) oxidation (Croal et al., 2004), abiotic Fe(II) oxidation and precipitation of ferric hydroxides (Bullen et al., 2001; Balci et al., 2006), and sorption of aqueous Fe(II) onto ferric hydroxides (Icopini et al., 2004; Teutsch et al., 2005). The largest equilibrium isotope fractionations of around 3‰ have been observed and theoretically calculated between co-existing Fe(III) and Fe(II) aqueous species (Johnson et al., 2002; Welch et al., 2003; Anbar et al., 2005).

Our knowledge of the Fe isotope composition of Fe sources to the ocean remains incomplete. Fe carried by rivers, including both soluble, colloidal and particulate fractions, has  $\delta^{56}\text{Fe}$  values ranging between  $\sim 0$  and  $-1$ ‰, suggesting that riverine Fe is isotopically light relative to igneous rocks (Fantle and DePaolo, 2004; Bergquist and Boyle, 2006). Iron isotope compositions of marine pore fluids from the California continental reveal a relatively large Fe isotope fractionation during early diagenetic processes, with  $\delta^{56}\text{Fe}$  values ranging from  $-3$  to  $+0.4$ ‰ (Severmann et al., 2006). Hence, the intense cycling of Fe between oxidized and reduced species in the upper few cm of coastal sediments can lead to the release of low  $\delta^{56}\text{Fe}$  iron from sediments to the water column (Staubwasser et al., 2005; Severmann et al., 2006).

Studies indicate that groundwater may contribute significantly to dissolved chemical species to the oceans (Moore, 1999) and, in one recent case, may also represent a large source of dissolved Fe to the coastal ocean (Windom et al., 2006). The magnitude of groundwater fluxes is influenced by biogeochemical processes occurring in the subterranean estuary, defined as the mixing zone between groundwater and seawater in a coastal aquifer. Dissolved Fe concentrations in subterranean estuaries, like their river-seawater counterparts, are strongly controlled by non-conservative (removal) behavior during mixing of river water and seawater (Sholkovitz, 1976; Boyle et al., 1977). However, a unique feature of subterranean estuaries is that the removal of Fe and other nutrients is mainly controlled by the redox characteristics of the fresh and saline groundwater (Slomp and VanCappellen, 2004). In particular, the recent discovery of an “Iron Curtain” in the subterranean estuary of Waquoit Bay on Cape Cod, USA demonstrates extensive precipitation of groundwater-borne dissolved ferrous iron and subsequent accumulation of iron oxides onto subsurface sands at the groundwater-seawater interface (Charette and Sholkovitz, 2002; Charette et al., 2005; Charette and Sholkovitz, 2006). Waquoit Bay is thus an excellent natural laboratory to assess the Fe-isotope composition of the groundwater input in a coastal zone and to evaluate if the iron flux from subterranean estuaries has a unique Fe isotope signature that is distinct from other coastal iron sources.

Here, we report a comprehensive study that demonstrates that the precipitation of iron oxides and redox-driven diagenetic reactions in subterranean estuaries produce large-scale variations of Fe isotopes in both sediments and pore water. This approach provides important constraints on the mechanisms of Fe-isotope fractionation

during Fe redox cycling. In particular, we aim to evaluate the relative effects of Fe-isotope fractionation associated with oxidative Fe precipitation vs. reductive Fe-dissolution pathways in a redox stratified environment.

## 2. MATERIALS AND SETTING

Waquoit Bay is a shallow estuary located on the south shoreline of Cape Cod, MA, USA. A significant portion of the freshwater input into the bay occurs as submarine discharge of groundwater (Charette et al., 2001) which is mostly restricted to a narrow ( $\sim 25$  m-wide) band along the head of the bay (Michael et al., 2003) (Fig. 1). Freshwater flowing downgradient from the water table may either discharge at the shore or flow directly under the beach into the sea. The hydraulic gradient that drives freshwater toward the sea along the fresh-saline groundwater interface also drives saltwater shoreward, creating a saltwater circulation cell (Michael et al., 2005; Moore, 1999). The hydraulic gradient is influenced by tides and rainfall, leading to hourly (Sholkovitz et al., 2003), seasonal (Michael et al., 2003), and interannual variability in groundwater discharge rates at this location. Topography also exerts a significant control on the location and flux of groundwater discharge at Waquoit Bay (Mulligan and Charette, 2006). While these factors can modulate the peak concentration and vertical/horizontal position of the dissolved Fe plumes in Waquoit Bay, six years of repeated sampling shows the same general features in the Fe distributions as reported in this paper (Charette et al., 2005).

Previous studies of the subterranean estuary of Waquoit Bay (Charette and Sholkovitz, 2002, 2006; Charette et al., 2005) have reported on element cycling of Fe, Mn, Ba, P and U in the permeable sediments and pore water. A series of sediment cores, ranging from 1.1 to 2.0 m in length were collected at the head of Waquoit Bay in April 2001 using a vibracoring technique (Charette and Sholkovitz, 2002). The pore water within the permeable sands of these cores drained away during the extrusion and sectioning activities. Hence, our solid phase data of Fe isotopes for these cores are not accompanied by pore-water data. Of the five recovered cores, Cores 2 and 3 have been selected for this study based on their location relative to the source of groundwater in the bay (Fig. 1). Core 2 is located near the piezometer transect A-A' in Fig. 1 whereas Core 3 is located near piezometer #4, about 50 m apart. The recovered lengths for cores 2 and 3 were 175 and 169 cm, respectively. The most outstanding visual feature of these cores is the color changes that occur over a transition zone of many tens of centimeters. Core 2 changes from gray to dark red coating at a depth of  $\sim 85$  cm; this color change reflects predominantly the deposition of ferrihydrite (64%) with goethite (26%) and lepidocrocite (10%). Core 3 changes from gray to red to orange at a depth of  $\sim 30$  cm and has the largest amount of lepidocrocite (19%) whereas goethite and ferrihydrite represent 44 and 37% respectively (Charette et al., 2005). We also analyzed two types of “background” sediments (1) surface beach sand from the head of Waquoit Bay near the coring sites, and (2) offsite sand collected from a Vineyard Sound beach located 10 km from Waquoit Bay.

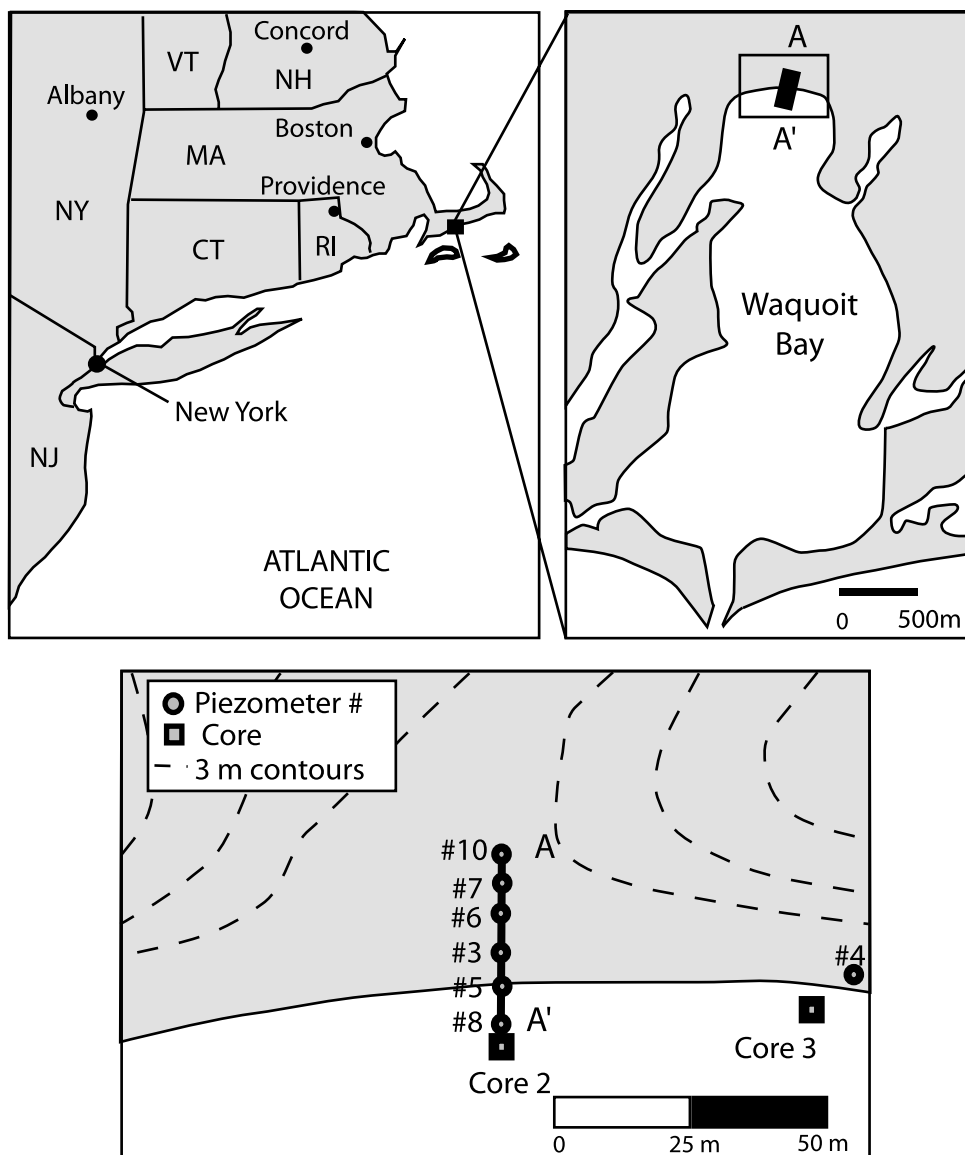


Fig. 1. Location of Waquoit Bay on Cape Cod, USA. The Bay opens to open seawater at the southern end. The expanded map of the head of the Bay shows the location of the piezometers along a profile (A-A') perpendicular to the shoreline. Location for piezometer #4 Core#2 and Core#3 are also presented.

173 All types of sediments (surface and deep) have similar size  
 174 distribution and contain greater than 95% sand (mainly  
 175 quartz with trace amounts of plagioclase and clinopyrox-  
 176 ene, amphiboles and mica) and less than 5% silt and clay.

177 A piezometer was used to obtain a two dimensional dis-  
 178 tribution of the porewater composition at the head of the  
 179 bay along a 17m transect. Field sampling methods and  
 180 porewater chemistry are presented in detail in previous  
 181 studies (Charette and Allen, 2006; Charette and Sholkovitz,  
 182 2006). The piezometer consists of a screened port at the end  
 183 of a thin probe which can be pushed down into the beach  
 184 sands. Ground water is pumped to the surface through  
 185 plastic tubing. Slow pumping and immediate filtration  
 186 using syringes keeps the ambient air out of the samples  
 187 which minimizes the oxidation of dissolved Fe (II) to par-

188 ticulate Fe (III) oxides prior to acidification and storage.  
 189 Each profile required 4 to 8 h of sampling, and the complete  
 190 transect covered 17 days (7 June to 3 July 2002). Hence, the  
 191 pore-water data do not represent synchronous distributions  
 192 of the measured parameters. The salinity distribution along  
 193 the piezometer transect A-A' (Fig. 1) is presented in Fig. 2  
 194 and shows that there is a well-defined subterranean estuary  
 195 beneath the head of the Bay. Fresh groundwater flows  
 196 across a narrow seepage face parallel to the shoreline.  
 197 Two distinct sources of high dissolved Fe have been identi-  
 198 fied (Fig. 2). One source resides in the upward rising plume  
 199 of Fe-rich freshwater and the second source lies in the salt-  
 200 wedge zone of mid to high salinity pore water. The second  
 201 source of dissolved Fe, where pore water concentrations  
 202 reach up to 75  $\mu\text{M}$  in Piezometer#8 along the transect A-

A' (Fig. 2) and up to 500  $\mu\text{M}$  in Piezometer #4 (~50 m away), result from chemical diagenesis typical of that found in reducing marine sediments where microbial activity leads to the reduction of Fe oxide (Froelich et al., 1979). Pore water data show that sulfate reduction is not occurring in the salt wedge section that contains high levels of reduced Fe and Mn. Hence, the production of sulfides is not an important part of the redox-driven cycling of Fe (Charette and Sholkovitz, 2006). The lack of sulfide formation in porewater, together with dissolved  $\text{O}_2$  concentration less down to 0.5 mg/L, suggest mostly  $\text{O}_2$ -deficient but not anoxic conditions within the subterranean estuary. Representative samples of groundwater and Fe(II)-rich pore waters with Fe concentration between 30 and 490  $\mu\text{M}$  were selected for Fe isotope measurements (Fig. 2).

It is important to note the large difference in scale between the sediment cores (maximum 1.8 m in length) and porewater samples that extend up to 8 m into the sediment beneath the head of Waquoit Bay (Fig. 2). Hence, sediment core geochemistry cannot be directly link to porewater geochemistry. Because the Fe concentrations continue to increase toward the bottom of the sediment cores, the full vertical extent of the iron curtain sediments was not entirely known at the time of collection. Recently, a set of longer (7 m) sediment cores from this location were collected. Fe (hydr)oxide analysis of the sediment revealed the existence of two iron curtains: (1) a shallow one, approximately 2 m in the vertical, likely associated with oxidation of Fe from the freshwater Fe plume, and (2) a deeper, 1 m zone of high Fe located just above the mid-high salinity Fe maximum (Gonneea et al., 2007).

### 3. ANALYTICAL METHOD

Core sediments and beach sands were air dried and hand-sieved through a polypropylene mesh with a nominal retention diameter of 1 mm. The concentration of Fe and Mn in the sieved sediments, along with their associated P, Ba, U and Th concentrations, have been reported previously (Charette et al., 2005; Charette and Sholkovitz, 2006) using a selective dissolution protocol (Hall et al., 1996). This protocol was designed to selectively dissolve “amorphous” iron oxides followed by “crystalline” Fe (hydr)oxides using reductive solutions of 0.25 M hydroxylamine hydrochloride in 0.05 M HCl and 1 M hydroxylamine hydrochloride in 25% glacial acetic acid respectively. The sum of these two leaches is referred to a “total oxide” composition and data are reported in Table 3.

Because reductive Fe-(hydr)oxides dissolution may fractionate Fe-isotopes during incomplete reduction of Fe(III) to Fe(II) (Icopini et al., 2004), we preferred using concentrated acid dissolution that prevent Fe-isotope fractionation (Skulan et al., 2002). Fe-oxides, coating quartz sands, were dissolved in PTFE beaker using ultra-pure grade 6N HCl on hot plate for 24 hours at approximately 80 °C. 10 mL of 6N HCl with 50  $\mu\text{L}$  of ultrapure  $\text{H}_2\text{O}_2$  were used for about 500 mg of sands. Because the sediments at Waquoit Bay are primarily composed of quartz sand coated with various Fe-oxide phases and contain only minor silicate minerals, Fe concentrations determined using our

strong acid leach method agreed well with total Fe concentration using the selective dissolution protocol reported in Charette et al. (2005). Sample purification for mass spectrometry analysis has been undertaken by ion-exchange chromatography in a clean room environment following previous protocols (Beard et al., 2003a; Rouxel et al., 2005). After centrifugation and separation of 6N HCl by pipetting, a precise solution volume, corresponding to not more than 100  $\mu\text{g}$  of Fe, was purified on Bio-Rad AG1X8 anion resin (2.5 mL wet bed). After 30 mL of 6N HCl was passed through the column to remove the matrix, 20 mL of 0.12N HCl was used to elute Fe. Eluted solution was then evaporated to dryness and dissolved with 2%  $\text{HNO}_3$  for mass spectrometry analysis.

In treating the pore water samples, aliquots are evaporated and then purified in the same manner as for solid samples. No more than 15 mL of the water samples are dried down in PTFE beakers with 1 mL of concentrated  $\text{HNO}_3$ . This step is repeated. The maximum operational volume for saline water reflects the high load of salts that prevent evaporating larger volume of waters without subsequent problems during chromatography separation. After evaporation, the residues of the water samples are dissolved with 5 mL 6N HCl with trace of  $\text{H}_2\text{O}_2$  and subsequently purified through ion-exchange chromatography.

The Fe isotope composition was determined with a Finnigan Neptune multicollector inductively coupled plasma mass spectrometry (MC-ICPMS) operated at Woods Hole Oceanographic Institution (WHOI). The Neptune instrument permits high precision measurement of Fe isotope ratios without argon interferences using high-mass resolution mode (Malinowski et al., 2003; Weyer and Schwiders, 2003; Arnold et al., 2004). Mass resolution power of about 8000 (medium resolution mode) was used to resolve isobaric interferences, such as ArO on  $^{56}\text{Fe}$ , ArOH on  $^{57}\text{Fe}$ , and ArN on  $^{54}\text{Fe}$ .

Instrumental mass bias is corrected using Ni isotopes as internal standard. This method, which has been proved to be reliable for the Neptune instrument, involves deriving the instrumental mass bias from simultaneously measuring a Ni standard solution (Malinowski et al., 2003; Poitrasson and Freyrier, 2005). We also used the “sample-standard bracketing” technique to correct for instrumental mass discrimination by normalizing Fe isotope ratios to the average measured composition of the standard that was run before and after the sample (Belshaw et al., 2000; Beard et al., 2003a; Rouxel et al., 2003). Fe isotope compositions are reported relative the Fe-isotope standard IRMM-14 using the following notation:

$$\delta^{56}\text{Fe} = 1000 * [({}^{56}\text{Fe}/{}^{54}\text{Fe})_{\text{sample}} / ({}^{56}\text{Fe}/{}^{54}\text{Fe})_{\text{IRMM-14}} - 1] \quad (1)$$

$$\delta^{57}\text{Fe} = 1000 * [({}^{57}\text{Fe}/{}^{54}\text{Fe})_{\text{sample}} / ({}^{57}\text{Fe}/{}^{54}\text{Fe})_{\text{IRMM-14}} - 1] \quad (2) \quad 311$$

$^{53}\text{Cr}$ ,  $^{54}\text{Fe}$ ,  $^{56}\text{Fe}$ ,  $^{57}\text{Fe}$ ,  $^{58}\text{Fe}$ +  $^{58}\text{Ni}$ ,  $^{60}\text{Ni}$ , and  $^{61}\text{Ni}$  isotopes were counted on the Faraday cups using the high mass resolution mode. Although quantitatively separated during analysis, Cr, which interferes with  $^{54}\text{Fe}$ , was monitored during each Fe isotope measurements and found to identical of background levels. Baseline corrections were made before acquisition of each data block by completely deflecting 318

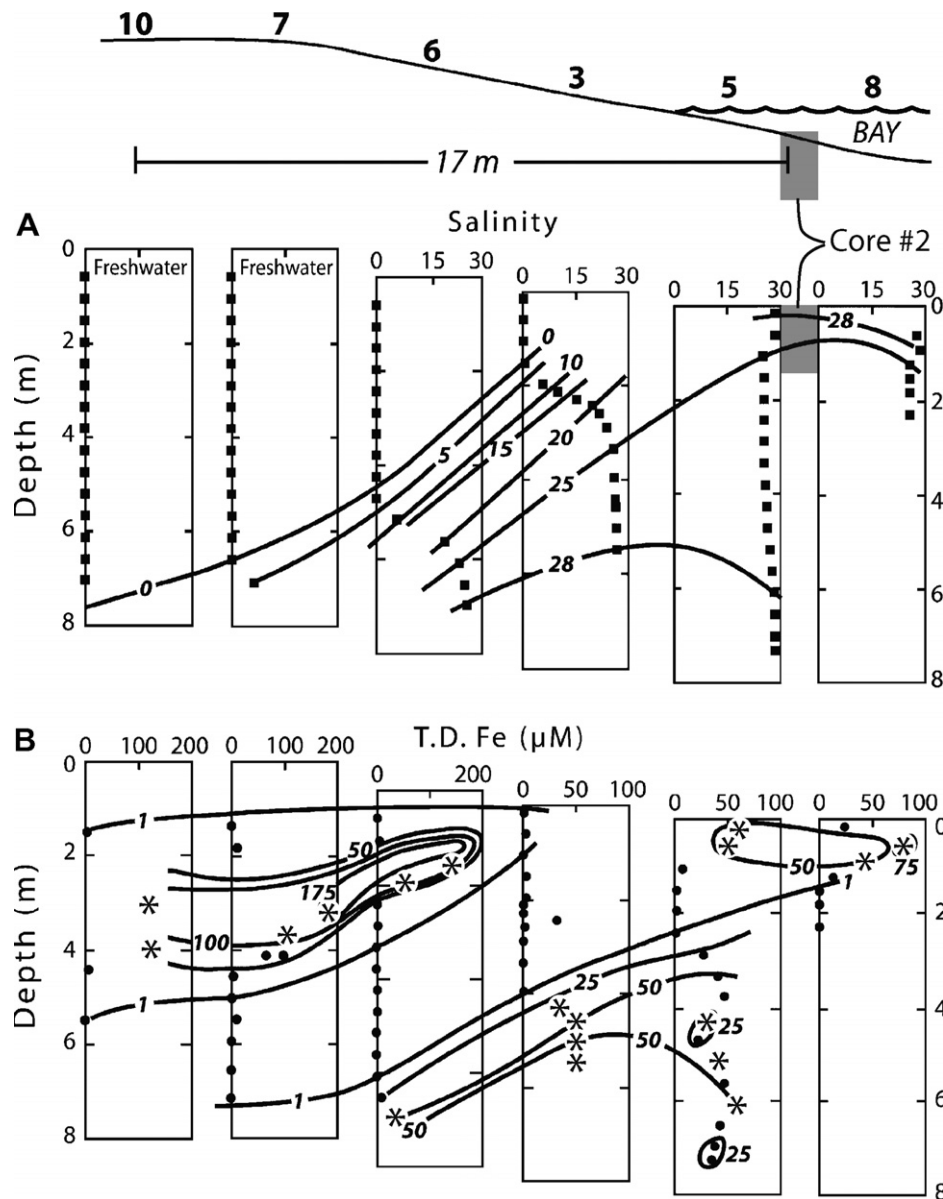


Fig. 2. Cross section of pore water salinity and total dissolve Fe concentration (T.D. Fe) in  $\mu\text{M}$  along the shore-perpendicular transect A-A' in Fig. 1. The isochores of constant salinity and and T.D. Fe and the corresponding Piezometer measurements from this study is shown in each box. The piezometer station numbers for each profile are located along the top edge of the figure. Locations of samples selected for Fe-isotope analysis are marked with "\*". Results for Piezometer#4 are not presented. Location and depth of Core #2 along the transect A-A' is also presented for comparison. Modified after Charette and Sholkovitz (2006).

319 the ion beam. All isotope data reported in this study were  
 320 analyzed at least twice using both techniques (i.e. Ni doping  
 321 and standard-sample bracketing) and the internal precision  
 322 of the data are given at 95% confidence levels based on the  
 323 standard deviation calculated on duplicates.

324 Purified samples of Fe-oxide-coated sands were diluted  
 325 to 1.5 ppm of Fe and Ni and introduced into the plasma  
 326 using a double quartz spray chamber system (cyclonic  
 327 and double pass) and a microconcentric PFA nebulizer  
 328 operating at a flow rate of about 100  $\mu\text{l}/\text{min}$ . Purified water  
 329 samples were analyzed using a desolvation nebulizer (Cetac  
 330 Apex) and X-cones (Thermo-Finnigan) to improve the sen-

sitivity of the *Neptune* (Schoenberg and von Blanckenburg,  
 2005).

331 Based on over 50 analyses – dissolution, purification and  
 332 ICP-MS measurement - of an internal standard (BHVO-1,  
 333 a Hawaiian basalt), we have obtained an average of  $\delta^{56}\text{Fe}$   
 334 values at 0.10 with a precision of 0.09‰ ( $2\sigma$ ). We evaluated  
 335 the accuracy of measuring Fe isotopes in saline water sam-  
 336 ples through the analysis of Fe isotope composition of arti-  
 337 ficial samples corresponding to seawater-like matrix doped  
 338 with Fe standard. Procedural blanks, including evapora-  
 339 tion/dissolution steps and ion exchange purification are be-  
 340 low 5 ng. As presented in Table 1, a precision of 0.15‰ can  
 341  
 342

Table 1

Fe-isotope composition of seawater matrix doped with various amount of Fe isotopic standards (IRMM-14 and BHVO-1)

Sample	Fe $\mu\text{M}$	N#	$\delta^{56}\text{Fe}$	2SD	$\delta^{57}\text{Fe}$	2SD
Seawater <sup>a</sup> Doped with IRMM-14						
#1	5	4	0.03	0.19	0.06	0.27
#2	5	2	0.08	0.17	0.12	0.21
#3	10	2	$\wedge$ -0.01	0.15	$\wedge$ -0.05	0.21
#4	10	2	0.05	0.02	0.11	0.01
Average			0.04	0.08	0.06	0.16
Seawater <sup>a</sup> Doped with BHVO-1						
#1	10	2	0.16	0.20	0.20	0.20
#2	20	2	0.04	0.05	0.05	0.12
#3	50	2	0.09	0.03	0.28	0.10
#4	200	2	0.06	0.09	0.16	0.17
#5	400	2	0.16	0.02	0.21	0.04
#6	600	2	0.07	0.15	0.10	0.21
Average			0.10	0.10	0.17	0.16

# Number of duplicated analysis used to calculate average Fe-isotope composition and precision (2SD: 2 standard deviation).

<sup>a</sup> Used 15 mL of seawater and processed through complete chemical purification procedure. Procedural blank (seawater only) determined at  $\sim 0.1 \mu\text{M}$ .

343 be achieved for saline water samples as low as  $5 \mu\text{M}$  and  
344 probably lower.

## 345 4. RESULTS

### 346 4.1. Fe-isotope composition of groundwater and brackish 347 porewaters

348 In a previous study, Charette and Sholkovitz (2006) re-  
349 ported Fe concentrations in porewater ranging from less  
350 than  $1 \mu\text{M}$  to up to  $500 \mu\text{M}$  for the whole salinity range  
351 of the subterranean estuary. A subset of twenty-six pore-  
352 water samples has been selected for this study based on  
353 their Fe concentration and location within the subterranean  
354 estuary. Exact location of these porewater samples relative  
355 to the subterranean estuary are presented in Fig. 2 together  
356 with corresponding Fe-concentration and salinity.

357 We selected groundwater samples with salinity  $< 0.4$   
358 along the piezometer transect (Pz #6, 7 and 10) to charac-  
359 terize the Fe-isotope composition of Fe(II) in the seaward-  
360 moving plume of freshwater feeding the subterranean estu-  
361 ary. Results show a range of  $\delta^{56}\text{Fe}$  values between 0.44 and  
362  $-0.8\text{‰}$  (Table 2) with higher  $\delta^{56}\text{Fe}$  values found in shal-  
363 lower sections whereas lower  $\delta^{56}\text{Fe}$  values are found deeper  
364 near the salinity gradient within the subterranean estuary.

365 We also selected brackish porewater samples with salin-  
366 ity between 19 and 29 and Fe-concentrations between 40  
367 and  $500 \mu\text{M}$  and obtained  $\delta^{56}\text{Fe}$  values ranging from  
368  $-4.8\text{‰}$  to  $0.22\text{‰}$  (Table 2). It is important to note that  
369 porewater having a salinity between 19 and 27 (e.g. Piezom-  
370 eter #3 and #4) display the largest Fe-isotope fractionation  
371 suggesting that most of the fractionation of Fe-isotopes in  
372 porewater is observed at the interface between the two ma-  
373 jor sources of reduced Fe in the subterranean estuary. This  
374 range of  $\delta^{56}\text{Fe}$  values is the largest reported so far in natural

375 systems and indicates that Fe redox cycling across the salin-  
376 ity gradient at Waquoit is able to produce extreme Fe-isot-  
377 ope fractionation in porewater.

### 378 4.2. Fe-isotope composition of permeable sediments

379 As presented in Fig. 3 and Table 3, Fe oxide coated  
380 sands in Core #2 have Fe concentrations ranging from  
381  $500$  to  $8000 \text{ ppm}$  and  $\delta^{56}\text{Fe}$  values decreasing upward from  
382  $\sim 1.5\text{‰}$  at  $140 \text{ cm}$  to  $0\text{‰}$  near the surface. The  $\delta^{56}\text{Fe}$  gradi-  
383 ent of  $1.5\text{‰}$ , over  $1.4 \text{ m}$  of section mirrors the Fe concentra-  
384 tion gradient. The Fe concentration in Core 3 increases  
385 downward from  $900 \text{ ppm}$  to more than  $7500 \text{ ppm}$  at  $100$   
386  $\text{cm}$ . In contrast to mostly positive  $\delta^{56}\text{Fe}$  values in Core 2,  
387 Core 3 oxides have systematically negative  $\delta^{56}\text{Fe}$  values.  
388 Core 3 also exhibits a well defined minimum  $\delta^{56}\text{Fe}$   
389 ( $-1.8\text{‰}$ ) in the mid-depth section ( $45\text{--}55 \text{ cm}$ ) while maxi-  
390 mum  $\delta^{56}\text{Fe}$  values (between  $-0.2$  and  $-0.4\text{‰}$ ) occur at  
391 the top and bottom ( $120 \text{ cm}$ ) of the core (Fig. 3). The over-  
392 all range of  $\delta^{56}\text{Fe}$  values  $\sim 1.6\text{‰}$  in Core 3 is however sim-  
393 ilar to Core 2. Two types of “background” sediments  
394 (surface beach sand at Waquoit Bay and offsite sand col-  
395 lected  $10 \text{ km}$  from Waquoit Bay) were also analyzed and re-  
396 sults show a restricted range of Fe-isotope composition  
397 clustered at  $0\text{‰}$  and Fe concentrations between  $300$  and  
398  $430 \text{ ppm}$ .

399 Because a vibra-core was used to recover sediment cores,  
400 it was not possible to sample corresponding pore water.  
401 Although Core 2 and 3 were recovered in the proximity  
402 of piezometer #8 and #4 respectively (Fig. 1), we only have  
403 Fe-isotope composition of pore water deeper in the section.  
404 However, we note that generally negative  $\delta^{56}\text{Fe}$  values in  
405 Fe-oxides in Core 3 (down to  $-1.8\text{‰}$ ) are consistent with  
406 the highly negative values found in Piezometer #4 ( $\delta^{56}\text{Fe}$   
407 values down to  $-2.4\text{‰}$  at  $4 \text{ meters}$  depth). Likewise, posi-  
408 tive  $\delta^{56}\text{Fe}$  values in Core 2 are consistent with higher  
409  $\delta^{56}\text{Fe}$  values in Piezometer #8 ( $\delta^{56}\text{Fe}$  between  $0.22$  and  
410  $-0.31\text{‰}$  from  $0.6$  to  $0.9 \text{ m}$  depth). Hence, the major differ-  
411 ence between Core 2 (i.e. mostly positive  $\delta^{56}\text{Fe}$  values) and  
412 Core 3 (i.e. mostly negative  $\delta^{56}\text{Fe}$  values) is, to a first  
413 approximation, the result of different initial  $\delta^{56}\text{Fe}$  values  
414 for pore water Fe(II) for each cores. The difference between  
415  $\delta^{56}\text{Fe}$  values in Core 2 and 3 that are about  $50 \text{ m}$  apart as  
416 well as the variability of  $\delta^{56}\text{Fe}$  values of up to  $1.5\text{‰}$  within  
417 each core demonstrate large variations of porewater  $\delta^{56}\text{Fe}$   
418 values over several centimeters to meters at the head of  
419 the Bay. The significance of these variations is discussed  
420 in the following section.

## 421 5. DISCUSSION

### 422 5.1. Freshwater source at Waquoit Bay

423 Cape Cod ground burden consists mainly of coarse-  
424 grained sand, and as such rain precipitation infiltrates the  
425 sediments and recharges subsurface aquifers. Hence,  
426 groundwater is a major source of freshwater to Waquoit  
427 Bay in addition to the two rivers that drain into it (Charette  
428 et al., 2001). The source of Fe(II) we have measured in the  
429 groundwater is uncertain, but likely derives from rainwater

Table 2  
Pore water concentrations of trace metals, Fe isotope composition of metals and ancillary water quality parameters

Depth (m)	Salinity	PO <sub>4</sub> (μM)	SiO <sub>4</sub> (μM)	Mn (μM)	U (nM)	Fe (μM)	N#	δ <sup>56</sup> Fe	2SD	δ <sup>57</sup> Fe	2SD
Piezometer #3											
4.42	25.9	4.6	222.0	22.8	12.5	39.7	4	-4.91	0.14	-7.38	0.19
4.57	26.1	6.9	214.0	21.4	10.30	50.6	2	-4.19	0.13	-6.28	0.18
5.03	26.4	13.1	190.0	8.4	8.5	50.6	4	-2.47	0.19	-3.63	0.15
5.49	26.6	15.8	161.0	4.2	7.70	51.0	2	-2.29	0.14	-3.32	0.20
Piezometer #4											
3.96	19.1	0.9	245.0	26.1	1.3	146.0	2	-2.43	0.03	-3.75	0.03
4.42	23.2	0.5	203.0	30.0	2.8	112.0	2	-1.68	0.18	-2.50	0.25
4.88	24.5	0.7	196.0	19.6	2.4	67.4	2	-1.36	0.19	-1.97	0.19
5.79	26.5	7.8	200.0	19.4	1.7	64.5	2	-1.13	0.16	-1.67	0.25
6.71	25.7	14.1	171.0	16.2	1.4	77.6	2	-0.79	0.08	-1.19	0.11
7.16	25.7	14.2	174.0	21.3	1.4	100.9	2	-0.53	0.18	-0.75	0.16
7.62	26.2	9.6	152.0	17.4	1.2	330.0	2	-0.36	0.10	-0.51	0.17
7.92	26.5	8.9	158.0	18.9	1	491.5	2	-0.37	0.18	-0.63	0.25
Piezometer #5											
0.15	28.8	9.4	83.4	14.1	4.3	58.9	2	-0.64	0.03	-0.93	0.03
0.61	28.8	9.4	121.0	23.6	3.3	48.4	2	-1.43	0.21	-2.18	0.30
5.18	27.5	13.1	141.0	2.6	3.9	42.6	2	-1.89	0.17	-2.80	0.16
5.64	28.1	10.3	138.0	2.8	2.7	46.7	2	-1.20	0.15	-1.79	0.19
6.55	28.9	14.3	102.0	1.4	2.5	41.5	2	-1.15	0.13	-1.82	0.16
Piezometer #6											
1.52	0.4	0.5	27.4	5.0	0.8	141.1	2	0.44	0.03	0.74	0.05
1.98	0.1	2.5	16.9	1.2	1.0	54.2	2	-0.10	0.12	-0.21	0.14
7.01	25.7	1.8	202.0	29.1	17.3	42.9	2	-2.03	0.13	-3.07	0.16
Piezometer #7											
3.20	0.0	0.7	117.0	2.7	1.2	196.3	2	-0.17	0.15	-0.26	0.19
3.66	0.0	0.1	109.0	12.9	0.1	106.5	4	-0.79	0.05	-1.14	0.05
Piezometer #8											
0.61	27.6	9.3	178.0	31.3	3.4	79.0	4	0.22	0.12	0.43	0.13
0.91	28.4	4.8	232.0	30.0	1.2	41.2	4	-0.31	0.14	-0.47	0.16
Piezometer #10											
3.05	0.0	0.2	23.5	3.0	0.3	119.4	3	0.29	0.12	0.45	0.21
3.96	0.0	0.1	25.1	4.7	1.5	128.3	4	-0.66	0.11	-0.89	0.15

PO<sub>4</sub>, SiO<sub>4</sub>, Mn, U and Fe data determined by high-resolution ICPMS from Charette and Sholkovitz, 2006.

# Number of duplicated analysis used to calculate average Fe-isotope isotope composition and precision (2SD: 2 standard deviation).

430 circulating through soils and local freshwater ponds. Previ-  
 431 ous measurements that have been made on dissolved Fe in  
 432 rivers, including both soluble and colloidal fractions, have  
 433 shown variable δ<sup>56</sup>Fe values ranging between ~0 and -1  
 434 ‰. This suggests that dissolved Fe is isotopically light rela-  
 435 tive to igneous rocks (Fantle and DePaolo, 2004; Bergquist  
 436 and Boyle, 2006). Measurements on the Fe-isotope compo-  
 437 sitions of pore water in soils also indicate that mineral dis-  
 438 solution in the presence of Fe-chelating organic ligands and  
 439 Fe-reducing bacteria preferentially releases light Fe from  
 440 silicates and Fe-oxides (Brantley et al., 2001; Brantley et  
 441 al., 2004; Emmanuel et al., 2005). Teutch et al. (2005) ob-  
 442 tained δ<sup>56</sup>Fe values of -0.4 ± 0.1‰ for anoxic groundwater  
 443 which are lighter than the sediment leach for Fe(III)  
 444 (0.16 ± 0.05 ‰). These values have been interpreted as  
 445 reflecting a slight fractionation (only 0.3 ‰) during micro-  
 446 bial mediated reductive dissolution of Fe-oxyhydroxides  
 447 present in the aquifer.

448 Our measurements of δ<sup>56</sup>Fe values in the groundwater at  
 449 Waquoit Bay, between 0.44 and -0.8‰, are thus similar to  
 450 the values that have been obtained for dissolved Fe in sev-  
 451 eral other systems. The lowest δ<sup>56</sup>Fe values down to -0.8‰  
 452 could be explained by either reductive dissolution of

Fe(III)-oxyhydroxides (Beard et al., 2003a; Icopini et al., 453  
 2004; Balci et al., 2006) or organic-ligand promoted silicate 454  
 dissolution (Brantley et al., 2004) in soil environments. The 455  
 origin of the positive δ<sup>56</sup>Fe values (up to 0.44‰) is however 456  
 less clear. It is possible that they are due to quantitative 457  
 reductive dissolution of isotopically enriched Fe-oxides in 458  
 subsurface sediments beneath the head of the Bay. It is also 459  
 possible that run-off freshwater may be characterized by 460  
 slightly positive δ<sup>56</sup>Fe values ~0.4 ‰ as recently reported 461  
 in local rivers (Escoube et al., 2007). In both cases, δ<sup>56</sup>Fe 462  
 values in groundwater are controlled by the mixing between 463  
 shallow and deeper sources with positive and negative δ<sup>56</sup>Fe 464  
 values respectively. Based on these results, we constrain the 465  
 δ<sup>56</sup>Fe value of the freshwater source of Fe(II) to Waquoit 466  
 Bay to be around -0.15 ± 0.5 ‰ which is, on average, close 467  
 to bulk δ<sup>56</sup>Fe values for soils and lithogenic Fe-sources 468  
 (Emmanuel et al., 2005; Poitrasson and Freyrier, 2005). 469

## 5.2. Fe-isotope systematics of Fe-oxide coated sands 470

471 As reported by Charette and Sholkovitz (2002), the dee-  
 472 per sections of Cores 2 and 3 are characterized by large  
 473 amounts of Fe oxides (ferrihydrite, lepidocrocite and goe-

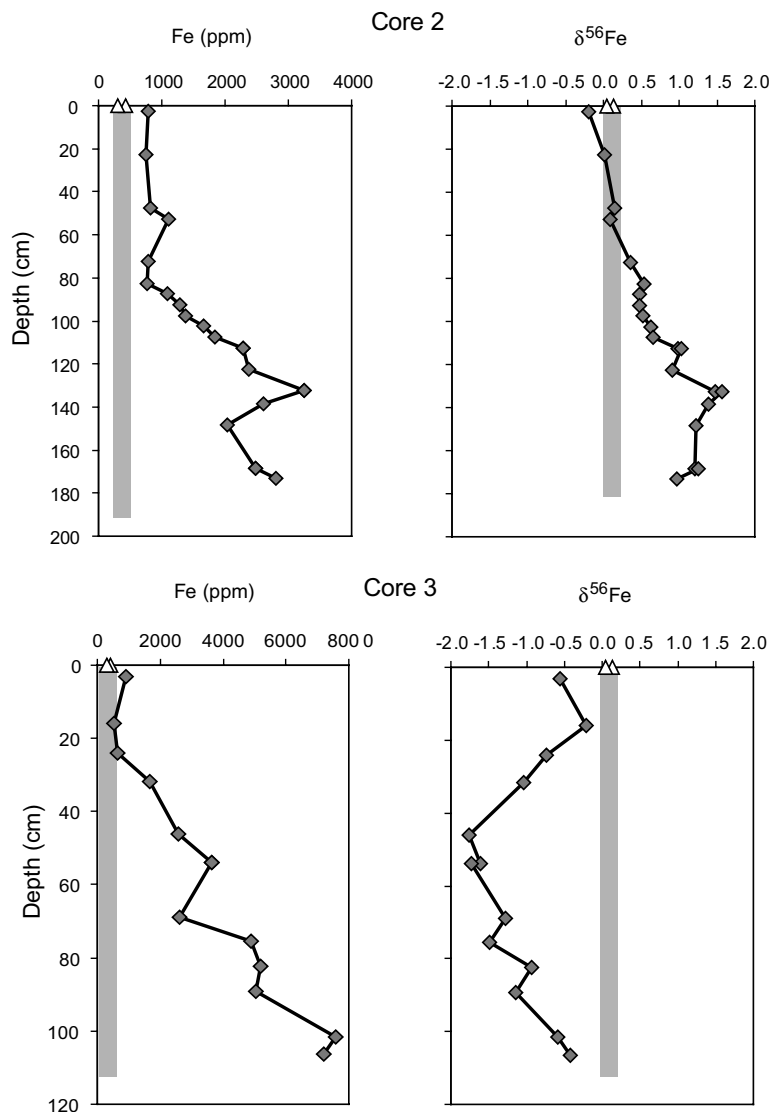


Fig. 3. Downhole variations of Fe-concentration and Fe-isotope composition in Fe-oxyhydroxide coated sands from A) Core#2 and B) Core#3. Core 2 and Core 3 are located in the tidal zone of the head of Waquoit Bay near piezometer #8 and #4 respectively (see Fig. 1). Gray shaded area correspond to the range of Fe-concentration and Fe-isotope composition for “off-site” surface beach sands reported in Table 1.

474 thite) that precipitate on quartz sand. Note that the salinity  
 475 gradient along Piezometers #8 and #4 is located in the  
 476 vicinity of Core 2 and 3 respectively (Table 2). This implies  
 477 that the source of Fe to these sediment cores is derived from  
 478 Fe(II)-rich brackish pore waters. A “background” Fe-oxy-  
 479 hydroxide component in sand is also anticipated in Core 2  
 480 and 3 because the analysis of two surface beach sand sam-  
 481 ples, away from any groundwater sources, yielded Fe con-  
 482 centration between 300 and 430 ppm (Table 3). This  
 483 “background” Fe-oxyhydroxide component has a restricted  
 484 range of Fe-isotope composition clustered at 0‰. Although  
 485 the source of Fe-oxyhydroxide in coastal area may be mul-  
 486 tiple (e.g. detrital, hydrogeneous, diagenetic sources), beach  
 487 sands remote from local groundwater sources tend to have  
 488 homogeneous Fe concentrations and  $\delta^{56}\text{Fe}$  values near 0‰.  
 489 Hence, two major components of Fe are expected in sedi-  
 490 ment Core 2 and 3: (1) background Fe-oxides with  $\delta^{56}\text{Fe}$

491 values near 0‰ and concentrations below 500ppm; and  
 492 (2) and Fe-oxides formed during the upward transport  
 493 and oxidation of Fe(II)-rich pore waters from saline zone.

494 An important question to address is whether these vari-  
 495 able  $\delta^{56}\text{Fe}$  values and Fe-concentrations through the sedi-  
 496 ment cores at Waquoit Bay result from mixing effects  
 497 between lithogenic Fe-oxides and diagenetic (i.e. derived  
 498 from Fe-rich porewater) Fe-oxides or result from *in-situ*  
 499 Fe-isotope fractionation during oxidative Fe precipitation.  
 500 The potential relationships between Fe concentrations  
 501 and  $\delta^{56}\text{Fe}$  values of Fe oxides in the case of mixing between  
 502 lithogenic and diagenetic Fe-oxides are presented in Fig. 4.  
 503 The model assumes  $\delta^{56}\text{Fe}$  values for lithogenic at 0‰ and  
 504 diagenetic Fe-oxides having  $\delta^{56}\text{Fe}$  values similar to those  
 505 measured in the deeper section of each core. The results  
 506 suggest that Fe-isotope composition of both sediment cores  
 507 cannot be simply explained by a binary mixing between

Table 3  
Chemical composition and Fe-isotope composition of surface beach sediment and sediment cores

Sample	Depth	Fe <sub>T</sub> ppm	Mn <sub>T</sub> ppm	N#	δ <sup>56</sup> Fe	2SD	δ <sup>57</sup> Fe	2SD
Surface beach sand from Waquoit Bay near the coring sites								
Sand "WB"	0.1	426	n.d.	2	0.04	0.17	0.13	0.27
<i>duplicate</i> <sup>a</sup>				2	−0.06	0.12	−0.07	0.14
<i>duplicate</i>				2	−0.03	0.10	0.00	0.15
Surface beach sand from Vineyard Bay, 10 km from Waquoit Bay								
Sand "PB"	0.1	303	1890	2	0.00	0.08	0.08	0.22
<i>duplicate</i>				2	0.06	0.10	0.10	0.20
<i>duplicate</i>				2	0.02	0.17	0.11	0.21
Sediment Core 2								
Core 2-1	2.5	785	23	3	−0.20	0.06	−0.30	0.02
Core 2-5	22.5	744	4	3	−0.01	0.19	−0.04	0.22
Core 2-10	47.5	820	4	3	0.14	0.09	0.29	0.17
Core 2-11	52.5	1106	5	2	0.09	0.04	0.16	0.04
Core 2-15	72.5	791	3	2	0.35	0.08	0.51	0.15
Core 2-17	82.5	772	4	2	0.54	0.05	0.75	0.14
Core 2-18	87.5	1094	5	4	0.48	0.24	0.70	0.32
Core 2-19	92.5	1279	7	2	0.48	0.07	0.67	0.17
Core 2-20	97.5	1373	9	6	0.52	0.21	0.78	0.34
Core 2-21	102.5	1666		2	0.63	0.01	0.93	0.01
Core 2-22	107.5	1847		2	0.65	0.02	0.96	0.01
Core 2-23	112.5	2279	12	3	0.98	0.06	1.42	0.14
<i>duplicate</i>				3	1.03	0.08	1.52	0.17
Core 2-25	122.5	2376		2	0.92	0.02	1.42	0.04
Core 2-28	132.5	3255	7	2	1.48	0.10	2.35	0.20
<i>duplicate</i>				2	1.57	0.14	2.40	0.18
Core 2-30	138.5	2613	5	2	1.39	0.04	2.09	0.10
Core 2-33	148.5	2040	5	2	1.22	0.02	1.75	0.04
Core 2-38	168.5	2480	6	2	1.20	0.01	1.81	0.01
<i>duplicate</i>				2	1.26	0.05	1.84	0.01
Core 2-41	173	2795	–	3	0.98	0.23	1.55	0.14
Sediment Core 3								
Core 3-17	3.2	906	9	4	−0.56	0.17	−0.83	0.29
Core 3-15	16.1	532	16	2	−0.21	0.14	−0.27	0.19
Core 3-14	24.2	659	5	2	−0.74	0.06	−1.06	0.03
Core 3-13	31.8	1684		2	−1.04	0.10	−1.52	0.11
Core 3-11	46.1	2581	11	3	−1.76	0.15	−2.60	0.16
Core 3-10	53.9	3625	15	3	−1.61	0.03	−2.34	0.06
<i>duplicate</i>				2	−1.70	0.16	−2.45	0.25
Core 3-8	69.0	2605		2	−1.27	0.03	−1.86	0.02
Core 3-7	75.6	4883	26	2	−1.49	0.00	−2.18	0.05
Core 3-6	82.4	5181	27	2	−0.93	0.05	−1.40	0.11
Core 3-5	89.3	5041	23	3	−1.14	0.09	−1.71	0.17
Core 3-3	101.7	7588	22	3	−0.58	0.17	−0.85	0.24
Core 3-2	106.4	7190	17	2	−0.42	0.03	−0.60	0.05

# Number of duplicated analysis used to calculate average Fe-isotope composition and precision (2SD: 2 standard deviation Fe and Mn concentration determined by reductive leaching method and ICPMS analysis, after Charette et al., 2006.

<sup>a</sup> *^ Duplicate* analysis include dissolution, chemical purification and mass spectrometry analysis.

508 these two sources. In the case of Core 2, the mixing between  
509 lithogenic and isotopically enriched Fe-oxides does not ac-  
510 count for the near linear correlation between Fe concentra-  
511 tions and δ<sup>56</sup>Fe values. Similarly, in the case for Core 3, the  
512 strong curvature observed between Fe concentrations and  
513 δ<sup>56</sup>Fe values argue against simple mixing effects.

514 The correlation between Fe concentration and δ<sup>56</sup>Fe val-  
515 ues in Core 2 and bottom half of Core 3 is consistent with  
516 results reported by Bullen et al. (2001) and Teutsch et al.  
517 (2005). Bullen et al. (2001) reported abiotic Fe isotope frac-  
518 tionation during precipitation of isotopically enriched Fe-  
519 oxyhydroxides from Fe-rich spring water, resulting in light-

er aqueous Fe(II) and lower Fe in the remaining dissolved 520  
Fe(II). Teutsch et al. (2005) measured the evolution of the 521  
Fe-isotope composition of Fe(II)-rich reduced groundwater 522  
during injection of oxygen-containing water. They show 523  
that the adsorption of Fe(II) onto newly formed Fe(III)- 524  
oxyhydroxides yields a very light groundwater component 525  
with δ<sup>56</sup>Fe values as low as −3 ‰, indicating that heavier 526  
Fe(II) is preferentially adsorbed to the newly formed 527  
Fe(III)-oxyhydroxides surfaces. These field observations 528  
are consistent with experimental studies showing a prefer- 529  
ential enrichment of heavy Fe-isotopes associated with the 530  
formation of Fe-oxyhydroxides (Welch et al., 2003; Croal 531

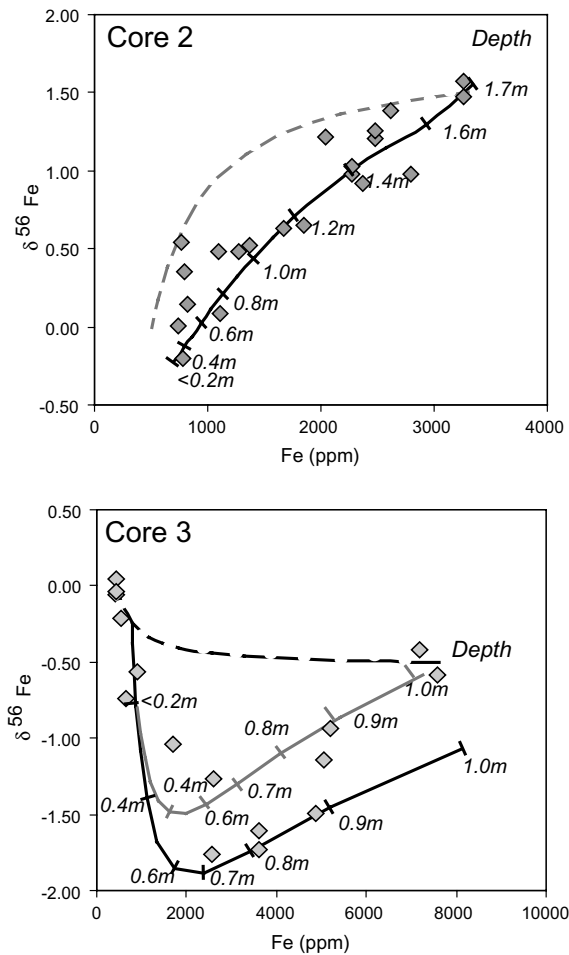


Fig. 4. Relationship between Fe-concentration and Fe-isotope composition of Fe-oxyhydroxide coated sands in Core 2 and 3. Simple mixing relationships between Fe-oxyhydroxide coated sands at the bottom of Core 2 and 3 and surface beach sands ( $[\text{Fe}] = 500 \text{ ppm}$ ,  $\delta^{56}\text{Fe} = 0 \text{ ‰}$ ) are illustrated using dashed lines. Gray and black lines correspond to the theoretical relationships between Fe concentration and Fe-isotope composition of sediments for each depth and are calculated using advection-reaction model during partial Fe(II) oxidation and Fe-oxyhydroxide precipitation. A) Model line for Core 2 is calculated using initial conditions for  $\delta^{56}\text{Fe} = 0.8 \text{ ‰}$ , Fe(II) oxidation rate of  $0.12 \text{ d}^{-1}$  and isotope fractionation factor  $\alpha = 1.001$ . B) Both model lines for Core 3 are calculated using initial conditions for  $\delta^{56}\text{Fe} = -0.8 \text{ ‰}$  and isotope fractionation factor  $\alpha = 1.0012$ . Gray line and black lines are calculated using Fe(II) oxidation rate of  $0.25 \text{ d}^{-1}$  and  $0.4 \text{ d}^{-1}$  respectively. See text and Appendix for discussion.

uppermost  $\sim 2 \text{ m}$  of sediments, limited by oxic coastal seawater and Fe(II)-rich porewater (Fig. 5). Hence, for each depth level, Fe concentration and isotope composition in sediments will be controlled by the extent of Fe-oxyhydroxide precipitation and input from underlying porewater as well as and the relative contribution of “background” Fe-oxides having  $\delta^{56}\text{Fe} = 0 \text{ ‰}$ . In this model, the theoretical relationship between Fe concentration and Fe-isotope composition of sediments for each depth is calculated using advection-reaction model during partial Fe(II) oxidation and Fe-oxyhydroxide precipitation. Variable parameters of this model include: i) initial  $\delta^{56}\text{Fe}$ ; composition of porewater Fe(II); ii) Fe(II) oxidation rate; iii) Fe-isotope fractionation factor  $\alpha$  between Fe(II) and Fe-oxyhydroxides. The rate of Fe(II) oxidation cannot be easily determined at each depth since  $\text{O}_2$  concentrations are not available along the sediment sections. Nevertheless, in the oxygen deficient conditions in sediment porewater of Waquoit Bay, with  $\text{O}_2 < 5 \text{ } \mu\text{M}$  and seawater-like pH, temperature and salinity, the Fe(II) oxidation rate is expected to be less than  $\sim 0.3 \text{ day}^{-1}$  (Millero et al., 1987). The mean ground-

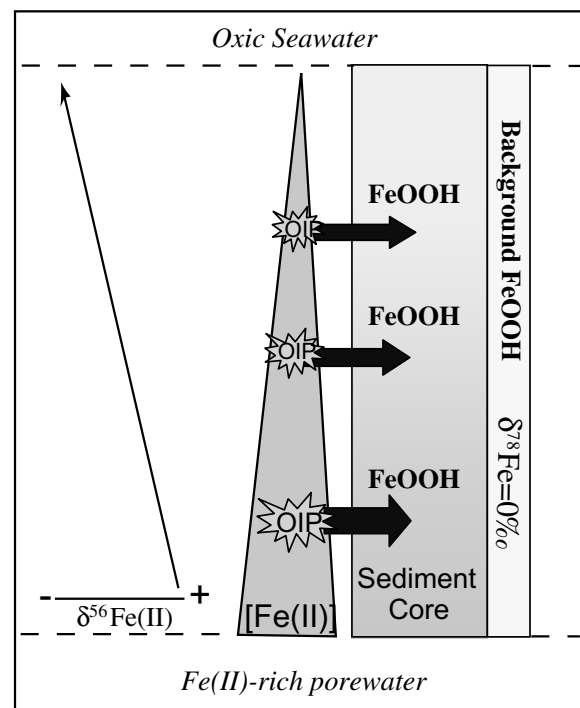


Fig. 5. Conceptual model used for calculating theoretical relationship between Fe-concentration and Fe-isotope composition observed in Fe-oxyhydroxide coated sands in Core 2 and 3. In this model, the upward transport and oxidation of Fe(II)-rich pore waters from saline zone and/or freshwater represents the major source of the Fe-oxyhydroxide rich cores. In addition, it is assumed that sands contain significant proportion of “background” Fe-oxides with  $\delta^{56}\text{Fe}$  near  $0 \text{ ‰}$  as demonstrated by the analysis of surface sands in area not affected by groundwater input (Table 1). During Oxidative Fe Precipitation (OIP), newly formed Fe-oxyhydroxide will preferentially incorporate heavy Fe-isotopes, producing a remaining aqueous Fe(II) pool enriched in light Fe-isotopes.

et al., 2004; Balci et al., 2006). Our results also suggest that a similar process is affecting the Fe-isotope composition of sediment cores at the head of Waquoit Bay.

In order to test the hypothesis that the fractionation of Fe-isotopes in iron oxides is controlled by partial oxidation of Fe(II)-rich porewater upon mixing with seawater, we have formulated a simple mathematical model for the evolution of Fe-isotopes in sediments. The numerical model is described in more detail in Appendix A and results are presented below for Core #2 and #3. In this model, it is considered that Fe(II) is progressively oxidized within the

564 water discharge for the head of Waquoit Bay is considered  
 565 constant at  $8 \text{ cm d}^{-1}$  following the estimation by Abraham  
 566 et al. (2003). It is however important to note that significant  
 567 temporal variability of the groundwater discharge occurs in  
 568 response to tidal cycles and seasonal or interannual precipi-  
 569 tation variability. There is also evidence that the ground-  
 570 water discharge is heterogeneously distributed along the  
 571 head of Waquoit Bay with Core 3 located in area with high-  
 572 er groundwater flow than in Core 2 (Mulligan and Char-  
 573 rette, 2006). Although a more complex numerical  
 574 treatment of Fe-isotope systematics in sediment cores, one  
 575 that integrates variable rates of Fe(II) oxidation, Fe-isotope  
 576 fractionation factors and groundwater discharge (both ver-  
 577 tically and horizontally) is possible, such a model is beyond  
 578 our objectives for this paper.

### 579 5.2.1. Core 2

580 Results for Core 2 are presented in Fig. 4 and show that  
 581 the relationship between Fe-concentration and Fe-isotope  
 582 composition can be modeled using a simple advection-reac-  
 583 tion model during partial Fe(II) oxidation and Fe-oxyhy-  
 584 droxide precipitation. A best fit of the data is obtained  
 585 using a solid-liquid fractionation factor ( $\alpha$ ) at 1.001 and ini-  
 586 tial  $\delta^{56}\text{Fe}$  values of  $0.8\text{‰}$ . The pseudo-first-order rate con-  
 587 stant of Fe(II) oxidation is set constant at  $0.12 \text{ d}^{-1}$  over  
 588 the entire core section, which is consistent with suboxic con-  
 589 ditions (Millero et al., 1987). The value around 1.001 for the  
 590 fractionation factor indicate that the  $\delta^{56}\text{Fe}$  value of precipi-  
 591 tated Fe-oxides is enriched in heavy isotopes by  $1.0\text{‰}$  rela-  
 592 tive to dissolved Fe(II) which is similar to those obtained  
 593 for abiotic Fe oxidation (around  $0.9\text{‰}$ ) (Bullen et al., 2001)  
 594 and slightly lower than for bacterial Fe oxidation (around  
 595  $1.5\text{‰}$ ) (Croal et al., 2004). The initial  $\delta^{56}\text{Fe}_i$  value  
 596 ( $\sim 0.8\text{‰}$ ) of porewater in Core 2 is however higher than  
 597 maximum measured  $\delta^{56}\text{Fe}$  values in porewater from Pie-  
 598 zometer #8 ( $\delta^{56}\text{Fe}$  between  $0.22$  and  $-0.31\text{‰}$  from  $0.6$  to  
 599  $0.9 \text{ m}$  depth). This discrepancy may be explained by the dif-  
 600 ferences in sampling time (i.e. Core 2 was recovered in April  
 601 2001 whereas porewater samples were recovered between  
 602 June and July 2002) and the fact that porewater composi-  
 603 tion may changes through time. It is also possible that high-  
 604 er porewater  $\delta^{56}\text{Fe}_i$  values ( $\sim 0.8\text{‰}$ ) are due to reductive  
 605 dissolution of isotopically enriched Fe-oxides previously  
 606 precipitated deeper in Core 2.

### 607 5.2.2. Core 3

608 Results for Core 3 are presented in Fig. 4 and the rela-  
 609 tionship between Fe-concentration and Fe-isotope compo-  
 610 sition has been modeled using a similar advection-reac-  
 611 tion model than for Core 2. Although the model repro-  
 612 duce the well defined minimum  $\delta^{56}\text{Fe}$  values ( $-1.5$  to  $1.8\text{‰}$ )  
 613 in the mid-depth section ( $0.5$ – $0.6 \text{ m}$ ), a single best-fit model  
 614 curve cannot be obtained using a constant Fe(II) oxidation  
 615 rate over the entire section of Core 3. Using a solid-liquid  
 616 fractionation factor ( $\alpha$ ) at 1.0012, the lower section of Core  
 617 2 is best explained using Fe(II) oxidation rate at  $0.25 \text{ d}^{-1}$   
 618 whereas the upper section is best explained using higher  
 619 Fe(II) oxidation rate at  $0.4 \text{ d}^{-1}$  (Fig. 4). These results sug-  
 620 gest that Fe(II) oxidation rate increase upward, during mix-  
 621 ing between  $\text{O}_2$ -poor porewater and oxic seawater.

622 It is interesting to note that, although Fe-isotope values  
 623 between Core 2 and 3 are different, similar process (i.e. par-  
 624 tial Fe(II) oxidation during upward advection of Fe-rich  
 625 porewater) can explain Fe-isotope values in both Cores.  
 626 In particular, the curvature in Fig. 4 between Fe concentra-  
 627 tion and  $\delta^{56}\text{Fe}$  values in Core 3 (i.e. minimum  $\delta^{56}\text{Fe}$  values  
 628 at mid-depth) is explained by the cumulative effect of (1)  
 629 preferential depletion in heavy Fe isotopes in porewater  
 630 due to partial oxidation, producing negative  $\delta^{56}\text{Fe}$  values  
 631 for Fe(III)-oxides and (2) increase in  $\delta^{56}\text{Fe}$  values for  
 632 Fe(III) due to mixing effects with “background” Fe-oxyhy-  
 633 droxides having  $\delta^{56}\text{Fe}$  values around  $0\text{‰}$ . Because the bot-  
 634 tom half of Core 3 has much higher Fe-oxide concentration  
 635 than “background” sands,  $\delta^{56}\text{Fe}$  values are mostly affected  
 636 by Fe-isotope fractionation during partial Fe(II) oxidation  
 637 whereas the top half, with lower Fe-oxide concentration,  
 638 suggest a prominent effect of physical mixture between  
 639 porewater-precipitated and “background” Fe-oxyhydrox-  
 640 ides. Similar mass balance consideration can be applied  
 641 for Core 2 to explain the lack of curvature between Fe con-  
 642 centration and  $\delta^{56}\text{Fe}$  values in Fig. 4. In this case, the pre-  
 643 cipitation of isotopically heavy Fe-oxyhydroxides at the  
 644 bottom of the core produces isotopically lighter, but not  
 645 strongly negative, Fe-oxyhydroxides at the top of the core.  
 646 Hence, the presence of “background” Fe-oxyhydroxides at  
 647  $\sim 0\text{‰}$  through Core 2 doesn't have significant effects on the  
 648 overall Fe concentration vs.  $\delta^{56}\text{Fe}$  relationship, except in  
 649 the uppermost section of the Core.

### 650 5.3. Fe-isotope composition of brackish porewaters

651 Because the variability of  $\delta^{56}\text{Fe}$  values in groundwater  
 652 (between  $0.44$  and  $-0.8\text{‰}$ ) is of second order compared  
 653 to the large range of  $\delta^{56}\text{Fe}$  values up to  $5\text{‰}$  in brackish  
 654 porewaters (i.e. salinity between 19 and 27) (Fig. 6), it is un-  
 655 likely that the variations of  $\delta^{56}\text{Fe}$  values in brackish pore-  
 656 water is controlled by groundwater Fe-isotope  
 657 composition. Charette and Sholkovitz (2006) and Spiteri  
 658 et al. (2006) showed that a major fraction of iron in the fer-  
 659 rous-rich groundwater is oxidized within the freshwater end  
 660 of subterranean estuary between Piezometers 6 and 3. In-  
 661 deed, pore water pumped from piezometer 3 at a depth of  
 662  $3 \text{ m}$  contained suspended yellow particles that are nearly  
 663 pure iron oxyhydroxides. Spiteri et al. (2006) investigated  
 664 the effect of  $\text{O}_2$  and pH gradients on Fe(II) oxidation rates  
 665 along a flow-line in the subterranean estuary of Waquoit  
 666 Bay. Results show that the observed  $\text{O}_2$  gradient is not  
 667 the main factor controlling oxidative precipitation. Rather  
 668 it was shown that the pH gradient at the mixing zone of  
 669 freshwater and seawater causes a  $\sim 7$ -fold increase in the  
 670 rate of Fe(II) oxidation. In contrast, the enrichment of  
 671 Fe(II) in the saline porewater end-member is the result of  
 672 diagenetic reactions and reductive dissolution of Fe(III)  
 673 oxides. Hence, we infer that the large Fe-isotope fraction-  
 674 ation across the salinity gradient is due to successive redox  
 675 reactions associated with the oxidative precipitation of dis-  
 676 solved ferrous Fe in the freshwater endmember and the  
 677 reductive dissolution of Fe oxides at higher salinity.

678 However, an important question remains is whether the  
 679 very low  $\delta^{56}\text{Fe}$  values in porewaters (between  $-2$  and  $-5\text{‰}$ )

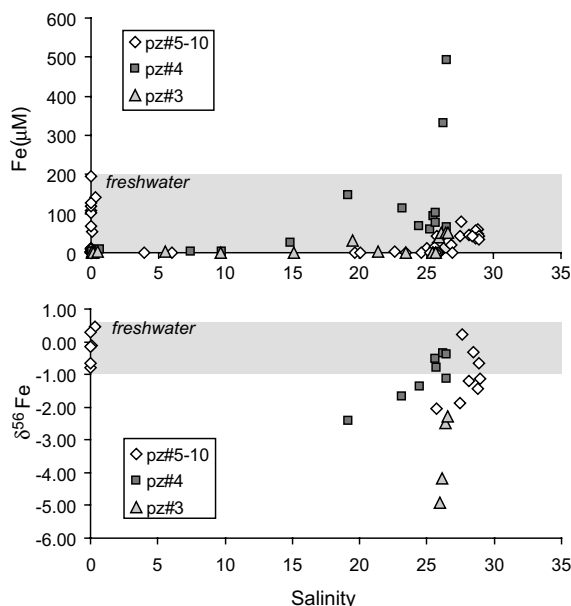


Fig. 6. Relationships between Fe-concentration and Fe-isotope composition relative to porewater salinity. Porewater along the transect A-A' (and specially related) are presented with the same symbol whereas porewater from piezometer 4 (50 m along shore) is presented separately. The source of dissolved Fe in high-salinity pore water concentrations (up to 500  $\mu\text{M}$ ) results from chemical diagenesis typical of that found in reducing marine sediments where microbial activity leads to the reduction of Fe oxide. Shaded area represents the range of Fe-concentration and isotope composition in freshwater source for Fe in the subterranean estuary.

680 are solely the result of diagenetic reduction of Fe-oxides or  
 681 may also result from partial Fe(II) oxidation in subsurface  
 682 environments, as previously demonstrated in Section 5.2 on  
 683 the sediment cores. It has been experimentally demon-  
 684 strated that Fe isotope fractionations during Fe(III) reduc-  
 685 tion (e.g. DIR, dissimilatory iron reduction) are dependent  
 686 on reduction rates (Beard et al., 2003a; Johnson et al., 2004;  
 687 Icopini et al., 2004). At high reduction rates, rapid forma-  
 688 tion and sorption of Fe(II) to ferric oxide substrate pro-  
 689 duced fractionations as large as  $-2.3\text{‰}$  but this value  
 690 corresponds to an extreme case. Hence, a fractionation of  
 691  $-1.3\text{‰}$  between biogenic Fe(II) and ferric oxide is more  
 692 representative. Our results of Fe-isotope composition of  
 693 saline porewaters ( $S > 27$ , Fig. 7) show  $\delta^{56}\text{Fe}$  values ranging  
 694 from 0.2 to  $-1.8\text{‰}$ , which are consistent with, but do not  
 695 necessarily prove, Fe-isotope fractionation by Fe-reducing  
 696 bacteria. These variations are also consistent with  $\delta^{56}\text{Fe}$   
 697 values found in suboxic porewater of margin sediments  
 698 (Staubwasser et al., 2005; Severmann et al., 2006) where  
 699 diagenetic Fe-redox cycling at sediment-water interface  
 700 produce isotopically depleted Fe(II) pool in porewater.  
 701 Porewater samples with the highest Fe concentrations  
 702 (Pz#4), representing the end-member for diagenetically re-  
 703 duced Fe(II), yield  $\delta^{56}\text{Fe}$  values of only  $-0.5\text{‰}$  which are  
 704 surprisingly similar to groundwater  $\delta^{56}\text{Fe}$  values (Fig. 7).  
 705 This minimal fractionation may reflect either small frac-  
 706 tionation factors during DIR due to specific environmental  
 707 conditions for Fe-reducing bacteria or either limiting

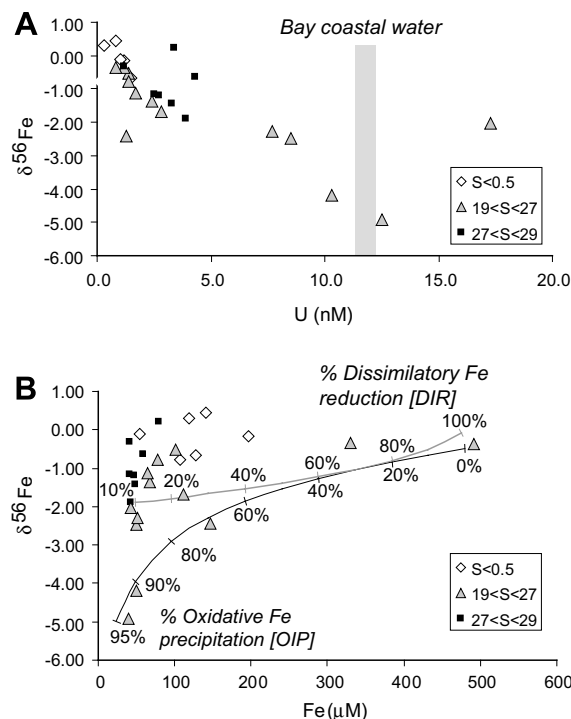


Fig. 7. A) and B) comparison of Fe-concentrations, Fe-isotope compositions and U concentrations in porewaters for different salinity. DIR = Dissimilatory Iron Reduction; OIP = Oxidative Iron Precipitation. A) U concentrations for local coastal seawater near Waquoit Bay are shown in comparison (data from Charette and Sholkovitz, 2006) and suggest that U, in most case, is removed under low  $\text{O}_2$  conditions in Waquoit Bay subterranean estuary. B) Example of  $\delta^{56}\text{Fe}$  vs. [Fe] relationships for DIR and OIP are shown for comparison. Initial reduction of ferric oxide substrate (i.e. open system reduction) produce  $\delta^{56}\text{Fe}$  values for Fe(II) down to  $-1.3\text{‰}$  and converge to initial Fe-isotope composition at high rate of DIR (i.e. close system reduction). OIP following Rayleigh-type distillation process is also presented. In this case, only large extent of Fe-oxidation will produce large Fe-isotope fractionation (down to  $-5\text{‰}$ ) in remaining aqueous Fe(II) pool.

708 Fe(III) substrate availability (i.e. quantitative reduction of  
 709 Fe(III) substrate). Considering the extent of Fe-isotope  
 710 fractionation during DIR at around  $-1.2$  to  $-1.5\text{‰}$  (Beard  
 711 et al., 2003a; Icopini et al., 2004), it appears unlikely that  
 712 DIR processes alone would produce  $\delta^{56}\text{Fe}$  values as low  
 713 as  $-5\text{‰}$  in porewaters in intermediate salinity and lower  
 714 Fe-concentrations.

715 Uranium in oxic sea water is very soluble as its redox  
 716 form is U(VI). In marked contrast, reducing conditions in  
 717 pore water and ground water lead to U(IV) which is very  
 718 particle reactive. Hence, reducing sediments are depleted  
 719 in pore water U; upon the return of more oxic conditions,  
 720 sedimentary U is oxidized to U(VI) species and U is rapidly  
 721 released in porewater (Barnes and Cochran, 1990). Because  
 722 soluble U(VI) can be converted to insoluble U(IV) under  
 723 conditions similar to those that favor the reduction of  
 724 Fe(III) to Fe(II) (Cochran et al., 1986; Barnes and Coch-  
 725 ran, 1990; Chaillou et al., 2002; McManus et al., 2006),  
 726 comparing U concentrations with  $\delta^{56}\text{Fe}$  values in porewa-  
 727 ters may provide insight regarding the relative effect of oxi-

728 dative Fe(II) precipitation vs. reductive Fe(III) dissolution.  
729 Charette and Sholkovitz (2006) reported U concentration  
730 in Waquoit subterranean estuary (Table 2) and observed  
731 a strongly non-conservative behavior of U with an overall  
732 net U removal over the entire salinity range. They also re-  
733 ported evidence for U increase above seawater values at  
734 the high salinity end which likely reflect the release of ad-  
735 sorbed U(IV) under more oxidizing conditions. As pre-  
736 sented in Fig. 7A, low  $\delta^{56}\text{Fe}$  values correlate well with  
737 high concentration of U in porewater. Assuming that sig-  
738 nificant oxidation of porewater Fe(II) and precipitation of  
739 Fe-oxyhydroxide are associated with U-rich pore waters,  
740 the low  $\delta^{56}\text{Fe}$  values (down to  $-5\text{‰}$ ) in the sediment cores  
741 can result from the precipitation of isotopically heavy Fe-  
742 oxyhydroxides rather than from the reductive dissolution  
743 of Fe-oxyhydroxides.

744 As illustrated in Fig. 7B, the oxidative Fe precipitation  
745 can explain the observed range of Fe(II) concentrations  
746 (from 500  $\mu\text{M}$  to 25  $\mu\text{M}$ ), as well as the Fe-isotopic compo-  
747 sition in porewater. The simple model presented in Fig. 7B  
748 assumes Rayleigh-type Fe-isotope fractionation in pore-  
749 water during oxidative Fe precipitation. Considering an ini-  
750 tial porewater Fe concentration of 500 $\mu\text{M}$  and  $\delta^{56}\text{Fe}$  value  
751 of  $-0.5\text{‰}$ ,  $\delta^{56}\text{Fe}$  values as low as  $-5\text{‰}$  would be expected  
752 after 95% of Fe-precipitation as Fe-oxyhydroxides with a  
753 fractionation factor of 1.0015 (Balci et al., 2006). Similar  
754 low  $\delta^{56}\text{Fe}$  values may be also obtained with smaller frac-  
755 tionation factors  $\sim 1.0012$  as those suggested during Fe(II)  
756 oxidation and precipitation of Fe-oxyhydroxides in sedi-  
757 ment cores, but requires lower initial  $\delta^{56}\text{Fe}$  values at around  
758  $-1.5\text{‰}$  (Fig. 7B). Additional fractionation is thus required  
759 if a significant fraction of precipitated Fe-oxides are further  
760 reduced and returned to the Fe(II) pool. For example, field  
761 observations suggest that redox gradients in Waquoit Bay  
762 groundwater are tightly coupled to seasonal and interan-  
763 nual movement of the fresh-saline groundwater interface  
764 (Charette et al., 2007).

765 Thus, multiple cycles of Fe-reduction and oxidation are  
766 likely to occur within the subterranean estuary at Waquoit  
767 Bay and can produce  $\delta^{56}\text{Fe}$  values down to  $-5\text{‰}$  in the  
768 porewaters. However, it is important to note that, though  
769 Fe reduction is responsible for the enrichment of Fe in  
770 porewater, strongly negative values of Fe-isotopes are  
771 mostly the result of the oxidative pathways of the Fe cycle  
772 and the sequestration of heavy Fe-isotopes in Fe-oxides. It  
773 is also possible that Fe(II) could be adsorbed onto newly  
774 formed Fe-oxyhydroxides in sediment during increasing  
775 oxygenation. Teutch et al. (2005) reported strong Fe-iso-  
776 tope fractionation (up to 3 $\text{‰}$ ) in groundwater Fe(II) result-  
777 ing from rapid adsorption of Fe(II) on Fe-oxyhydroxides  
778 formed during injection of  $\text{O}_2$ -containing water. Similar  
779 process may also be important in the subterranean estuary  
780 at Waquoit Bay given the high Fe-oxyhydroxide content in  
781 cores.

782 Fe-isotope results in the subterranean estuary of Wa-  
783 quoit Bay could be also compared to recent studies of Fe-  
784 isotope composition in Fe-oxide concretion from the Nava-  
785 jo Sandstone that precipitated from reducing Fe-rich  
786 groundwater (Chan et al., 2006; Busigny and Dauphas,  
787 2007). In these studies, negative  $\delta^{56}\text{Fe}$  values for Fe-oxide

788 concretions (down to  $\sim -2\text{‰}$ ) have been explained by com-  
789 plete oxidation and precipitation from aqueous fluids that  
790 had negative  $\delta^{56}\text{Fe}$  values. These low  $\delta^{56}\text{Fe}$  values have  
791 been either interpreted as resulting from bacterial reduction  
792 of Fe-oxides (Chan et al., 2006) or evolution of the fluid  
793 composition through precipitation and/or adsorption isoto-  
794 pically heavy Fe during fluid flow (Busigny and Dauphas,  
795 2007). These studies can be reconciled if both bacterial  
796 reduction of Fe-oxides and partial Fe(II) oxidation occur  
797 in conjunction in  $\text{O}_2$ -depleted environments, as those ob-  
798 served at Waquoit Bay.

#### 5.4. Hydrogeochemical model 799

800 The conceptual model of Fe-isotope systematic in sub-  
801 terranean estuary at Waquoit Bay is presented in the sche-  
802 matic diagram in Fig. 8. This figure incorporates the  
803 hydrology of the subterranean estuary as described previ-  
804 ously (Charette et al., 2005; Charette and Sholkovitz,  
805 2006) as well as Fe-isotope compositions observed in this  
806 study. Seepage meter studies at Waquoit Bay have shown  
807 that subterranean circulation leads to the upward flow of  
808 saline pore water to the intertidal zone (Michael et al.,  
809 2003; Sholkovitz et al., 2003). A plume of seaward flowing  
810 fresh groundwater and recirculating seawater lead to a salt-  
811 wedge type distribution of pore-water salinity. The sedi-  
812 mentary and aqueous environment of this subterranean  
813 estuary is one of active redox reactions for Fe where two  
814 major sources and oxidative sinks of reduced iron are  
815 found: (1) a freshwater plume from the land transporting  
816 high concentrations of dissolved Fe(II) toward the bay  
817 where the precipitation of iron oxyhydroxides occurs in  
818 the freshwater end of the plume (resulting from oxic sea-  
819 water recirculation and/or pH increase); and (2) the upward  
820 transport and oxidation of Fe(II)-rich pore waters in the  
821 saline zone (representing the major source of the iron oxy-  
822 hydroxide rich cores reported in this study). These terres-  
823 trial and marine sources are probably interconnected as  
824 they operate within several meters of each other in the ver-  
825 tical and offshore directions. Since both end-members have  
826  $\delta^{56}\text{Fe}$  values varying between 0.3 and  $-1.3\text{‰}$ , likely result-  
827 ing from dissimilatory Fe reduction (noted as DIR in Fig.  
828 8), most of the Fe-isotope fractionation is occurring during  
829 oxidative precipitation of Fe-oxyhydroxide (noted as OIP  
830 in Fig. 8) within the mixing zone between groundwater  
831 and brackish  $\text{O}_2$ -depleted porewater. Hence, both high con-  
832 centration of Fe(II) in porewater (resulting from DIR) and  
833 partial Fe(II) oxidation are required to produce the large  
834 scale Fe-isotope fractionation found in both sediment and  
835 porewater.

836 It is likely that this large-scale Fe isotope fractionation  
837 (up to 5 $\text{‰}$ ) produced by the precipitation of Fe-oxides in  
838 permeable sediments during the mixing of anoxic ground-  
839 water with seawater is not restricted to the subterranean  
840 estuary at Waquoit Bay. More generally, any coastal aquif-  
841 er with pore water bearing high dissolved ferrous iron that  
842 intercepts oxic to suboxic seawater may produce a Fe(II)  
843 flux to coastal seawater characterized by negative  $\delta^{56}\text{Fe}$  val-  
844 ues. The radium isotope studies by Charette et al. (2001)  
845 show that there is strong groundwater signature in Waquoit

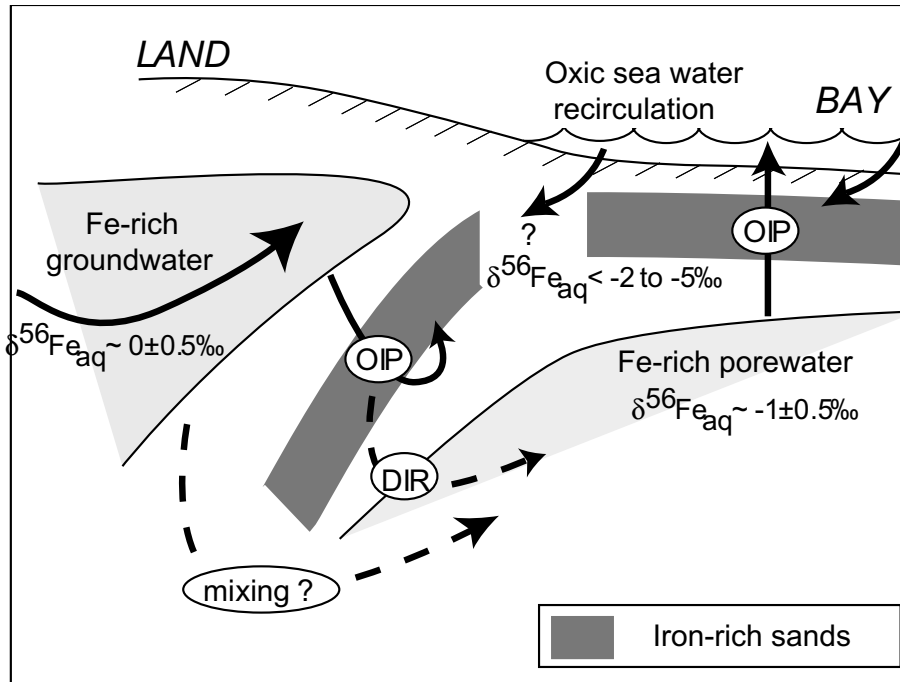


Fig. 8. Conceptual hydrogeochemical model at Waquoit Bay across a section perpendicular to transect A-A' in Fig. 1. This model integrates porewater Fe concentrations profile presented in Fig. 2 with high Fe(II) concentration represented as light-gray domain. Fe-oxide-rich sands (referred as "iron curtain") are represented as dark gray area. Oxidative Fe precipitation (OIP) and dissimilatory Fe reduction (DIR) processes are also presented to illustrate possible pathways of Fe-reduction and oxidation between different Fe reservoirs.

846 Bay water. Although the isotopic composition of dissolved  
847 and suspended Fe in the water column of Waquoit Bay  
848 has yet to be measured, our results imply that subterranean  
849 estuary may impact Fe-isotope budget in coastal waters.

## 850 6. CONCLUSIONS

851 Dissolved Fe has a distinctly non-conservative behavior  
852 in estuaries (Sholkovitz, 1976; Boyle et al., 1977; Mayer,  
853 1982) due to the rapid flocculation of dissolved Fe and humic  
854 substances during mixing between rivers and seawater.  
855 Similar features are also observed in subterranean estuaries  
856 but here, redox characteristics of the freshwater and seawater  
857 have significant influence on the partitioning of Fe between  
858 the solid and aqueous phases. In previous studies,  
859 it has been demonstrated that the upward transport of  
860 Fe(II)-rich groundwater is responsible for the formation  
861 of Fe oxide-rich sands (Iron Curtain) in the subterranean  
862 estuary of Waquoit Bay (Charette and Sholkovitz, 2002).  
863 In this study, we reported a large scale Fe isotope fractionation  
864 in iron-coated sands and porewater in the intertidal  
865 zone of Waquoit Bay. The distribution of Fe-isotopes in  
866 pore water reveal that very low  $\delta^{56}\text{Fe}$  values of porewater  
867 down to  $-5\%$  occur within the mixing zone of the subterranean  
868 estuary. We interpret the Fe-isotope fractionation  
869 to reflect intensive Fe-redox cycling across a density interface  
870 between anoxic groundwater and  $\text{O}_2$ -deficient saline  
871 porewaters. Large range of  $\delta^{56}\text{Fe}$  values, between  $-2$  and  
872  $1.5\%$  has been also observed in two sediment cores across  
873 the subterranean estuary. The relationship between Fe concentration  
874 and  $\delta^{56}\text{Fe}$  values of Fe oxides can be modeled by

incremental processes (distillation) during the progressive  
precipitation of Fe-oxides during fluid flow across the subterranean  
estuary. These results suggest that partial Fe(II) oxidation in low  $\text{O}_2$   
conditions is the major process producing the large scale Fe-isotope  
fractionation found in both sediment and porewater.

The Fe isotope composition of dissolved Fe in oceanic water masses  
has not been systematically determined as the analytical difficulties  
have yet to be mastered. Hydrogenous accumulations in the form of  
ferromanganese (Fe-Mn) oxides display variable, but negative  
 $\delta^{56}\text{Fe}$  values that may provide record of marine Fe isotope composition  
(Zhu et al., 2000; Lévassieur et al., 2004). Among potential sources  
of negative  $\delta^{56}\text{Fe}$  components in seawater, continental run-off  
(Fantle and DePaolo, 2004), hydrothermal sources (Beard et al.,  
2003b) and diagenetic pore fluids from shelf sediments (Staubwasser  
et al., 2005; Severmann et al., 2006) have been suggested to provide  
significant source of low- $\delta^{56}\text{Fe}$  iron to the oceans. In this study,  
we demonstrated that groundwater input in subterranean estuaries  
may also represent a significant source of light Fe in seawater due  
to the preferential sequestration of heavy Fe-isotopes in sediments,  
yielding aqueous Fe(II) with  $\delta^{56}\text{Fe}$  down to  $-5.0\%$ . Considering the  
recently recognized importance of submarine groundwater input as  
source of dissolved Fe in the ocean (Windom et al., 2006), future  
studies will need to focus on the Fe isotopic composition of coastal  
waters in order to further our understanding of the links between  
biogeochemical processes occurring in subterranean estuaries and  
coastal water Fe pools.

## ACKNOWLEDGMENTS

This study was supported by the National Science Foundation (OCE 0550066) to OR and ES, (OCE 0095384) to MC and ES and NASA Astrobiology Institute - Cycle 3 CAN-02-OSS-02 to KJE. Lary Ball is thanked for his technical support on the Neptune MC-ICPMS at WHOI. We thank Silke Severmann, Derek Vance, Tim Lyons and two anonymous reviewers for helpful comments on the manuscript.

## APPENDIX A

The model runs as follows. First, pore water  $Fe^{2+}$  concentrations within the uppermost 2m of the sediments are determined using the general 1-dimension diagenetic model described by Richter and DePaolo (1987) and Berner (1980):

$$\frac{\partial Ci}{\partial t} = Dc \frac{\partial^2 Ci}{\partial z^2} - v \frac{\partial Ci}{\partial z} + \sum R \quad (a.1)$$

where  $Ci$  represents the concentration of the solute  $i$ ,  $t$  is the time,  $z$  is the depth,  $Dc$  is the diffusivity of the solute  $i$ ,  $v$  is the advective velocity and  $\sum R$  represents the sum of the reaction terms.

In the case of homogeneous Fe(II)-oxidation in porewater,  $\sum R$  is given by

$$\sum R = -k1[Fe(II)] \quad (a.2)$$

where  $k1$  is the pseudo-first-order rate constant of Fe(II) oxidation which is strongly dependent upon pH and  $O_2$  (e.g. Millero et al., 1987) following:

$$k1 = -k[OH^-][O_2] \quad (a.3)$$

To a first approximation, this formulation does not take into account the heterogeneous oxidation whereby the rate of oxidation increases with the concentration of Fe(III) hydroxide due to autocatalytic effects.

The diffusion coefficient  $Dc$  is related to the temperature, porosity and tortuosity of the sediment which are considered constant with depth over the uppermost 2-m of sediment section. Given a porosity of 0.35 for sand sediments at Waquoit Bay (Hoefel and Evans, 2001),  $D_{Fe^{2+}}$  can be estimated at  $\sim 0.04 \text{ cm}^2 \text{ d}^{-1}$  (Li and Gregory, 1974). The groundwater discharge for the head of Waquoit Bay has been estimated by Abraham et al. (2003) at  $v \sim 8 \text{ cm d}^{-1}$ . Although the total groundwater discharge proceeds through both horizontal and vertical transport, we only considered vertical advection in our model. Because only two cores have been investigated in this study, it is presently impossible to develop a more complex 2D advection-reaction model.

This suggests that  $Fe^{2+}$  transport through the sediments is essentially advective (i.e. Peclet number  $\gg 1$ ) and that Eq. (a.1) could be simplified as:

$$\frac{\partial Fe^{2+}}{\partial t} = -v \frac{\partial Fe^{2+}}{\partial z} - k1[Fe^{2+}] \quad (a.4)$$

Since Fe(II) oxidation fractionate Fe-isotopes toward heavy isotopes in the insoluble Fe(III) product, the rate of Fe(II) oxidation is different between Fe-isotopes and Eq. (a.4) can be written for  $^{56}Fe$  and  $^{54}Fe$  isotopes:

$$\frac{\partial ^{56}Fe^{2+}}{\partial t} = -v \frac{\partial ^{56}Fe^{2+}}{\partial z} - ^{56}k1[^{56}Fe^{2+}] \quad (a.5)$$

$$\frac{\partial ^{54}Fe^{2+}}{\partial t} = -v \frac{\partial ^{54}Fe^{2+}}{\partial z} - ^{54}k1[^{54}Fe^{2+}] \quad (a.6)$$

Where  $^{54}k1$  and  $^{56}k1$  are the pseudo-first-order rate constant of  $^{54}Fe(II)$  and  $^{56}Fe(II)$  oxidation respectively. It is also assumed no differences in advection rate  $v$  between  $^{54}Fe$  and  $^{56}Fe$  isotopes.

The isotope fractionation factor during Fe(II) oxidation  $\alpha$  which is generally determined between 1.001 and 1.0015 (Bullen et al., 2001; Croal et al., 2004; Balci et al., 2006) is defined by

$$\alpha = ^{56}k1 / ^{54}k1 \quad (a.7)$$

The theoretical relationship between  $Fe^{2+}$  concentration and isotope composition in porewater can be calculated using the DuFort-Frankel scheme, an explicit three-level finite difference method (DuFort and Frankel, 1953; Richter and DePaolo, 1987). This model is stepped in time and space allowing for advection and reaction.  $Fe^{2+}$  concentration and  $^{56}Fe/^{54}Fe$  isotope ratios are calculated for each depth intervals using equations (4) and (5). The evolution of  $Fe_{t,z}^{2+}$  at time  $t$  and depth  $z$  is described by

$$\frac{Fe_{t+1,z}^{2+} - Fe_{t-1,z}^{2+}}{2\Delta t} = -v \frac{Fe_{t,z+1}^{2+} - Fe_{t,z-1}^{2+}}{2\Delta z} - k1 [Fe_{t-1,z}^{2+}] \quad (a.8)$$

The parameter  $\Delta t$  is the time step used in the model calculation (in day) while  $\Delta z$  is the grid spacing in cm. Similarly,  $^{54}Fe_{t,z}^{2+}$  and  $^{56}Fe_{t,z}^{2+}$  are calculated using the same centered finite approach for solving Eqs. (a.5) and (a.6).

Since Fe-oxidation product is insoluble and considered immobile in sediments, Fe(III) concentration can be calculated for each depth intervals, such as:

$$\frac{\partial Fe(III)}{\partial t} = k1[Fe^{2+}] \frac{\Phi}{\rho(1-\Phi)} \quad (a.9)$$

Where  $\rho$  is sediment density ( $\sim 2 \text{ g cm}^{-3}$ ) and  $\Phi$  sediment porosity of  $\sim 0.35$  for sediments at Waquoit Bay.

The evolution of  $^{54}Fe(III)$  and  $^{56}Fe(III)$  at time  $t$  and depth  $z$  is then described by:

$$\frac{^{56}Fe(III)_{t+1,z} - ^{56}Fe(III)_{t-1,z}}{2\Delta t} = k1 \frac{\Phi}{\rho(1-\Phi)} [^{56}Fe_{t-1,z}^{2+}] \quad (a.10)$$

$$\frac{^{54}Fe(III)_{t+1,z} - ^{54}Fe(III)_{t-1,z}}{2\Delta t} = \frac{k1}{\alpha} \frac{\Phi}{\rho(1-\Phi)} [^{54}Fe_{t-1,z}^{2+}] \quad (a.11)$$

Where we solve  $^{54}Fe(III)_{t+1,z}$  and  $^{56}Fe(III)_{t+1,z}$  and allow the determination of  $\delta^{56}Fe$  values of Fe-oxides at any depth  $z$ . The model is run until Fe(III) concentrations reaches the present day. Only parameters  $k1$  (rate of  $Fe^{2+}$  oxidation) and fractionation factor  $\alpha$  are adjusted to give a best fit of Fe(III) vs.  $\delta^{56}Fe$  relationship.

## REFERENCES

- Abraham D. R., Charette M. A., Allen M. C., Rago A. and Kroeger K. D. (2003) Radiochemical estimates of submarine groundwater discharge to Waquoit Bay, Massachusetts. *Bio. Bull.* **205**, 246–247.

- 1014 Anbar A. D., Jarzecki A. A. and Spiro T. G. (2005) Theoretical  
1015 investigation of iron isotope fractionation between  $\text{Fe}(\text{H}_2\text{O})_6^{3+}$   
1016 and  $\text{Fe}(\text{H}_2\text{O})_6^{2+}$ : Implications for iron stable isotope geochem-  
1017 istry. *Geochim. Cosmochim. Acta* **69**, 825–837.
- 1018 Anbar A. D. and Rouxel O. (2007) Metal Stable Isotopes in  
1019 Paleocyanography. *Annu. Rev. Earth Planet. Sci* **35**, 717–746.
- 1020 Archer D. E. and Johnson K. (2000) A model of the iron cycle in  
1021 the ocean. *Global Biogeochemical Cycles* **14**, 269–279.
- 1022 Arnold G. L., Weyer S. and Anbar A. D. (2004) Fe Isotope  
1023 variations in natural materials measured using high mass  
1024 resolution multiple collector ICPMS. *Anal. Chem.* **76**, 322–327.
- 1025 Balci N., Bullen T. D., Witte-Lien K., Shanks W. C., Motelica M.  
1026 and Mandernack K. W. (2006) Iron isotope fractionation  
1027 during microbially stimulated Fe(II) oxidation and Fe(III)  
1028 precipitation. *Geochim. Cosmochim. Acta* **70**, 622–639.
- 1029 Barnes C. E. and Cochran J. K. (1990) Uranium removal in  
1030 oceanic sediments and the oceanic U balance. *Earth Planet. Sci.*  
1031 *Lett.* **97**, 94–101.
- 1032 Beard B. L., Johnson C. M., Cox L., sun H., Neelson K. H. and  
1033 Aguilar C. (1999) Iron Isotope Biosignatures. *Science* **285**,  
1034 1889–1892.
- 1035 Beard B. L., Johnson C. M., Skulan J. L., Neelson K. H., Cox L.  
1036 and Sun H. (2003a) Application of Fe isotopes to tracing the  
1037 geochemical and biological cycling of Fe. *Chemical Geology*  
1038 **195**, 87–117.
- 1039 Beard B. L., Johnson C. M., VonDamm K. L. and Poulson  
1040 R. L. (2003b) Iron isotope constraints on Fe cycling and  
1041 mass balance in oxygenated Earth oceans. *Geology* **31**, 629–  
1042 632.
- 1043 Belshaw N. S., Zhu X. K., Guo Y. and O’Nions R. K. (2000) High  
1044 precision measurement of iron isotopes by plasma source mass  
1045 spectrometry. *International Journal of Mass Spectrometry and*  
1046 *Ion Processes* **197**, 191–195.
- 1047 Bergquist B. and Boyle E. (2006) Iron isotopes in the Amazon river  
1048 system: weathering and transport signatures. *Earth Planet. Sci.*  
1049 *Lett.* **248**, 54–68.
- 1050 Berner R. A. (1980) *Early Diagenesis: A Theoretical Approach*.  
1051 Princeton University Press, Princeton, NJ.
- 1052 Boyd P. W., Watson A. J., Law C. S., Abraham E. R., Trull T.,  
1053 Murdoch R., Bakker D. C. E., Bowie A., Buesseler K. O.,  
1054 Chang H., Charette M., Croot P., Downing K., Frew R., Gall  
1055 M., Hadfield M., Hall J., Harvey M., Jameson G., DeLaRoche  
1056 J., Liddicoat M., Ling R., Maldonado M. T., McKay R. M.,  
1057 Nodder S., Pickmere S., Pridmore R., Rintoul S., Safi K.,  
1058 Sutton P., Strzepek R., Tanneberger K., Turner S., Waite A.  
1059 and Zeldis J. (2000) A mesoscale phytoplankton bloom in the  
1060 polar Southern Ocean stimulated by iron fertilization. *Nature*  
1061 **407**, 695–702.
- 1062 Boyle E. A., Bergquist B. B., Kayser R. and Mahowald N. (2005)  
1063 Iron, manganese, and lead at Hawaii Ocean Time-series Station  
1064 ALOHA: Temporal Variability and an Intermediate Water  
1065 Hydrothermal Plume. *Geochim. Cosmochim. Acta* **69**, 933–952.
- 1066 Boyle E. A., Edmond J. M. and Sholkovitz E. R. (1977) The  
1067 mechanism of iron removal in estuaries. *Geochim. Cosmochim.*  
1068 *Acta* **41**, 1313–1324.
- 1069 Brantley B. L., Liermann L. J., Guynn R. L., Anbar A., Icopini G.  
1070 A. and Barling J. (2004) Fe isotopic fractionation during  
1071 mineral dissolution with and without bacteria. *Geochim. Cos-*  
1072 *mochim. Acta* **68**, 3189–3204.
- 1073 Brantley S. L., Liermann L. and Bullen T. D. (2001) Fractionation  
1074 of Fe isotopes by soil microbes and organic acids. *Geology* **29**,  
1075 535–538.
- 1076 Buck K. N., Lohan M. C., Berger C. J. M. and Bruland K. W.  
1077 (2007) Dissolved iron speciation in two distinct river plumes  
1078 and an estuary: Implications for riverine iron supply. *Limnol.*  
1079 *Oceanogr.* **52**, 843–855.
- Bullen T. D., White A. F., Childs C. W., Vivit D. V. and Schulz M. 1080  
S. (2001) Demonstration of significant abiotic iron isotope  
1081 fractionation in nature. *Geology* **29**, 699–702. 1082
- Busigny V. and Dauphas N. (2007) Tracing paleofluid circulations 1083  
using iron isotopes: A study of hematite and goethite concre- 1084  
tions from the Navajo Sandstone (Utah, USA). *Earth. Planet.* 1085  
*Sci. Lett.* **254**, 272–287. 1086
- Chaillou G., Anschutz P., Lavaux G., Schafer J. and Blanc G. 1087  
(2002) The distribution of Mo, U, and Cd in relation to major 1088  
redox species in muddy sediments of the Bay of Biscay. *Marine* 1089  
*Chemistry* **80**, 41–59. 1090
- Chan M. A., Johnson C. M., Beard B. L., Bowman J. R. and Parry 1091  
W. T. (2006) Iron isotopes constrain the pathways and 1092  
formation mechanisms of terrestrial oxide concretions: A tool 1093  
for tracing iron cycling on Mars. *Geosphere* **2**, 324–332. 1094
- Charette M. A. and Allen M. C. (2006) Precision Ground Water 1095  
Sampling in Coastal Aquifers Using a Direct-Push, Shielded- 1096  
Screen Well-Point System. *Ground Water Monitoring & Reme-* 1097  
*diation* **26**(2), 87–93. 1098
- Charette M. A., Buesseler K. O. and Andrews J. E. (2001) Utility of 1099  
radium isotopes for evaluating the input and transport of 1100  
groundwater-derived nitrogen to a Cape Cod estuary. *Limnol.* 1101  
*Oceanogr.* **46**, 465–470. 1102
- Charette M. A. and Sholkovitz E. R. (2002) Oxidative precipitation 1103  
of groundwater-derived ferrous iron in the subterranean estuary 1104  
of a coastal bay. *Geophysical Research Letters*, **29**. doi:10.1029/  
2001GL014512. 1105
- Charette M. A. and Sholkovitz E. R. (2006) Trace element in a 1107  
subterranean estuary: Part 2. Geochemistry of pore water. 1108  
*Geochim. Cosmochim. Acta* **70**, 811–826. 1109
- Charette M. A., Sholkovitz E. R. and Hansel C. M. (2005) Trace 1110  
element cycling in a subterranean estuary: Part 1. Geochemistry 1111  
of the permeable sediments. *Geochim. Cosmochim. Acta* **69**, 1112  
2095–2109. 1113
- Cochran J. K., Carey A. E., Sholkovitz E. R. and Surprenant L. D. 1114  
(1986) The geochemistry of uranium and thorium in coastal 1115  
marine sediments and sediment pore waters. *Geochem. Cosmo-* 1116  
*chim. Acta* **50**, 663–680. 1117
- Croal L. R., Johnson C. M., Beard B. L. and Newman D. K. 1118  
(2004) Iron isotope fractionation by Fe(II)-oxidizing photo- 1119  
autotrophic bacteria. *Geochimica et Cosmochimica Acta* **68**, 1120  
1227–1242. 1121
- Crosby H. A., Roden E. E., Johnson C. M. and Beard B. L. (2007) 1122  
The mechanisms of iron isotope fractionation produced during 1123  
dissimilatory Fe(III) reduction by *Shewanella putrefaciens* and 1124  
*Geobacter sulfurreducens*. *Geobiology* **5**, 169–189. 1125
- de Jong J., Schoemann V., Tison J.-L., Becquevort S., Masson F., 1126  
Lannuzel D., Petit J., Choua L., Weis D. and Mattielli N. 1127  
(2007) Precise measurement of Fe isotopes in marine samples by 1128  
multi-collector inductively coupled plasma mass spectrometry 1129  
(MC-ICP-MS). *Analytica Chimica Acta* **589**, 105–119. 1130
- DuFort E. C. and Frankel S. P. (1953) Stability conditions in the 1131  
numerical treatment of parabolic differential equations. *Math-* 1132  
*ematical Tables and Other Aids to Computation* **7**, 135–152. 1133
- Elderfield H. and Schultz A. (1996) Mid-ocean ridge hydrothermal 1134  
fluxes and the chemical composition of the ocean. *Annu. Rev.* 1135  
*Earth Planet. Sci.* **24**, 191–224. 1136
- Elrod V. A., Berelson W. M., Coale K. H. and Johnson K. S. 1137  
(2004) The flux of iron from continental shelf sediments: A 1138  
missing source for global budgets. *Geophysical Research Letters* 1139  
**31**. doi:10.1029/2004GL020216. 1140
- Emmanuel S., Erel Y., Matthews A. and Teutsch N. (2005) A 1141  
preliminary mixing model for Fe isotopes in soils. *Chemical* 1142  
*Geology* **222**, 23–34. 1143
- Escoube, R., Rouxel, O., Sholkovitz, E., Donard, O., 2007. Iron 1144  
Isotope Composition of River Water During Estuarine Mixing: 1145

- 1146 Case of North River (Massachusetts, USA). *Eos Trans. AGU*,  
1147 88(52), Fall Meet. Suppl., Abstract H31C-0513.
- 1148 Fantle M. S. and DePaolo D. J. (2004) Iron isotopic fractionation  
1149 during continental weathering. *Earth Planet. Sci. Lett.* **228**,  
1150 547–562.
- 1151 Froelich P. N., Klinkhammer G. P., Bender M. L., Luedtke N. A.,  
1152 Heath G. R., Cullen D., Dauphin P., Hammond D., Hartman  
1153 B. and Maynard V. (1979) Early oxidation of organic matter in  
1154 pelagic sediments of the eastern equatorial Atlantic: suboxic  
1155 diagenesis. *Geochimica et Cosmochimica Acta* **43**, 1075–1090.
- 1156 Hall G. E. M., Vaive J. E., Beer R. and Hoashi M. (1996) Selective  
1157 leaches revisited, with emphasis on the amorphous Fe oxyhy-  
1158 droxide phase extraction. *J. Geochem. Explor.* **56**, 59–78.
- 1159 Hoefel F. G. and Evans R. L. (2001) Impact of low salinity  
1160 porewater on seafloor electromagnetic data: a means of  
1161 detecting submarine groundwater discharge? *Estuarine, Coastal  
1162 and Shelf Science* **52**, 179–189.
- 1163 Hutchins D. A., Witter A. E., Butler A. and Luther, III, G. W.  
1164 (1999) Competition among marine phytoplankton for different  
1165 chelated iron species. *Nature* **400**, 858–861.
- 1166 Icopini G. A., Anbar A. D., Ruebush S. S., Tien M. and Brantley S.  
1167 L. (2004) Iron isotope fractionation during microbial reduction  
1168 of iron: The importance of adsorption. *Geology* **32**, 205–208.
- 1169 Jickells T. D., An Z. S., Andersen K. K., Baker A. R., Bergametti  
1170 G., Brooks N., Cao J. J., Boyd P. W., Duce R. A., Hunter K.  
1171 A., Kawahata H., Kubilay N., laRoche J., Liss P. S., Maho-  
1172 wald N., Prospero J. M., Ridgwell A. J., Tegen I. and Torres R.  
1173 (2005) Global Iron Connections Between Desert Dust, Ocean  
1174 Biogeochemistry, and Climate. *Science* **308**, 67–71.
- 1175 Johnson C. M., Beard B. L., Roden E. E., Newman D. K. and  
1176 Nealson K. H. (2004) Isotopic constraints on biological cycling  
1177 of Fe. *Reviews in Mineralogy and Geochemistry* **55**, 359–408.
- 1178 Johnson C. M., Skulan J. L., Beard B. L., Sun H., Nealson K. H.  
1179 and Braterman P. S. (2002) Isotopic fractionation between  
1180 Fe(III) and Fe(II) in aqueous solutions. *Earth Planet. Sci. Lett.*  
1181 **195**, 141–153.
- 1182 Johnson K. S., Chavez F. P. and Friederich G. E. (1999)  
1183 Continental-shelf sediment as a primary source of iron for  
1184 coastal phytoplankton. *Nature* **398**, 697–700.
- 1185 Levasseur S., Frank M., Hein J. R. and Halliday A. N. (2004) The  
1186 global variation in the iron isotope composition of marine  
1187 hydrogenetic ferromanganese deposits: implications for seawater  
1188 chemistry? *Earth and Planetary Science Letters* **224**, 91–105.
- 1189 Li Y.-H. and Gregory S. (1974) Diffusion of ions in sea water and  
1190 in deep-sea sediments. *Geochem. Cosmochim. Acta* **38**, 703–714.
- 1191 Malinowski D., Stenberg A., Rodushkin I., Andren H., Ingri J.,  
1192 Ohlander B. and Baxter D. C. (2003) Performance of high  
1193 resolution MC-ICPMS for Fe isotope ratio measurements in  
1194 sedimentary geological materials. *Journal of Analytical Atomic  
1195 Spectrometry* **18**, 687–695.
- 1196 Martin J. H. (1990) Glacial-interglacial CO<sub>2</sub> change: the iron  
1197 hypothesis. *Paleoceanography* **5**, 1–13.
- 1198 Mayer L. M. (1982) Retention of riverine iron in estuaries.  
1199 *Geochim. Cosmochim. Acta* **46**, 1003–1009.
- 1200 McManus J., Berelson W. M., Severmann S., Poulson R. L.,  
1201 Hammond D. E., Klinkhammer G. P. and Holm C. (2006)  
1202 Molybdenum and uranium geochemistry in continental margin  
1203 sediments: Paleoproxy potential. *Geochim. Cosmochim. Acta* **70**,  
1204 4643–4662.
- 1205 Michael H. A., Lubetsky J. S. and Harvey C. F. (2003) Charac-  
1206 terizing submarine groundwater discharge: A seepage meter  
1207 study in Waquoit Bay, Massachusetts. *Geophysical Research  
1208 Letters* **30**. doi:10.1029/2002GL016000.
- 1209 Michael H. A., Mulligan A. E. and Harvey C. F. (2005) Seasonal  
1210 oscillations in water exchange between aquifers and the coastal  
1211 ocean. *Nature* **436**, 1145–1148.
- 1212 Millero F. J., Sotolongo S. and Izaguirre M. (1987) The oxidation  
1213 kinetics of Fe(II) in seawater. *Geochimica et Cosmochimica Acta*  
1214 **51**, 793–801.
- 1215 Moore W. S. (1999) The subterranean estuary: a reaction zone of  
1216 groundwater and seawater. *Marine Chemistry* **65**, 111–125.
- 1217 Mulligan A. E. and Charette M. A. (2006) Intercomparison of  
1218 submarine groundwater discharge estimates from a sandy  
1219 unconfined aquifer. *Journal of Hydrology* **327**, 411–425.
- 1220 Poitrasson F. and Freyrier R. (2005) Heavy iron isotope compo-  
1221 sition of granites determined by high resolution MC-ICP-MS.  
1222 *Chemical Geology* **222**, 132–147.
- 1223 Powell R. T. and Wilson-Finelli A. (2003) Importance of organic  
1224 Fe complexing ligands in the Mississippi River plume. *Estuar-  
1225 ine, Coastal and Shelf Science* **58**, 757–763.
- 1226 Richter F. M. and DePaolo D. J. (1987) Numerical-models for  
1227 diagenesis and the Neogene Sr isotopic evolution of seawater  
1228 from DSDP Site 590B. *Earth Planet. Sci. Lett.* **83**, 27–38.
- 1229 Rouxel O., Bekker A. and Edwards K. (2005) Iron Isotope  
1230 Constraints on the Archean and Paleoproterozoic Ocean Redox  
1231 State. *Science* **307**, 1088–1091.
- 1232 Rouxel O., Dobbek N., Ludden J. and Fouquet Y. (2003) Iron  
1233 Isotope Fractionation During Oceanic Crust Alteration (Site  
1234 ODP 801). *Chem. Geol.* **202**, 155–182.
- 1235 Schoenberg R. and von Blanckenburg F. (2005) An assessment of  
1236 the accuracy of stable Fe isotope ratio measurements of samples  
1237 with organic and inorganic matrices by high-resolution multi-  
1238 collector ICP-MS. *Int. J. Mass Spectrom.*
- 1239 Severmann S., Johnson C. M., Beard B. L. and McManus J. (2006)  
1240 The effect of early diagenesis on the Fe isotope compositions of  
1241 porewaters and authigenic minerals in continental margin  
1242 sediments. *Geochimica et Cosmochimica Acta* **70**, 2006–2022.
- 1243 Sholkovitz E., Herbold C. and Charette M. (2003) An automated  
1244 dye-dilution based seepage meter for the time-series measure-  
1245 ment of submarine groundwater discharge. *Limnol. Oceanogr.*  
1246 *Methods* **1**, 16–28.
- 1247 Sholkovitz E. R. (1976) Flocculation of dissolved organic and  
1248 inorganic matter during the mixing of river water and seawater.  
1249 *Geochimica et Cosmochimica Acta* **40**, 831–845.
- 1250 Skulan J. L., Beard B. L. and Johnson C. M. (2002) Kinetic  
1251 and equilibrium Fe isotope fractionation between aqueous  
1252 Fe(III) and hematite. *Geochimica et Cosmochimica Acta* **66**,  
1253 2995–3015.
- 1254 Slomp C. P. and VanCappellen P. (2004) Nutrient inputs to the  
1255 coastal ocean through submarine groundwater discharge:  
1256 controls and potential impact. *Journal of Hydrology* **295**, 64–86.
- 1257 Spiteri C., Regnier P., Slomp C. P. and Charette M. A. (2006) pH-  
1258 Dependent iron oxide precipitation in a subterranean estuary.  
1259 *Journal of Geochemical Exploration* **88**, 399–403.
- 1260 Staubwasser M., Schoenberg R. and vonBlanckenburg F. (2005)  
1261 Fe-isotope fractionation during early diagenetic Fe-reduction.  
1262 *Geophysical Research Abstracts* **7**, 09176.
- 1263 Teutsch N., vonGunten U., Porcelli D., Cirpka O. A. and Halliday  
1264 A. N. (2005) Adsorption as a cause for Iron Isotope fractiona-  
1265 tion in reduced groundwater. *Geochim. Cosmochim. Acta* **17**,  
1266 4175–4185.
- 1267 Ussher S., Worsfold P. J., Achterberg E. P., Laës A., Blain S., Laan  
1268 P. and deBaar H. J. W. (2007) Distribution and redox  
1269 speciation of dissolved iron on the European continental  
1270 margin. *Limnol. Oceanogr.* **52**, 2530–2539.
- 1271 Welch S. A., Beard B. L., Johnson C. M. and Braterman P. S.  
1272 (2003) Kinetic and equilibrium Fe isotope fractionation  
1273 between aqueous Fe(II) and Fe(III). *Geochimica et Cosmochi-  
1274 mica Acta* **67**, 4231–4250.
- 1275 Wells M. L., Price N. M. and Bruland K. W. (1995) Iron chemistry  
1276 in seawater and its relationship to phytoplankton: a workshop  
1277 report. *Marine Chemistry* **48**, 157–182.

- 1278 Weyer S. and Schwieters J. B. (2003) High precision Fe isotope 1286  
1279 measurements with high mass resolution MC-ICPMS. *Internat-* 1287  
1280 *ional Journal of Mass Spectrometry* **226**, 355–368. 1288
- 1281 Windom H. L., Moore W. S., Niencheski L. F. H. and 1289  
1282 Jahnke R. A. (2006) Submarine groundwater discharge: 1290  
1283 A large, previously unrecognized source of dissolved iron 1291  
1284 to the South Atlantic Ocean. *Marine Chemistry* **102**, 252– 1292  
1285 266. 1293
- Wu J., Boyle E., Sunda W. and Wen L.-S. (2001) Soluble and 1286  
colloidal iron in the Oligotrophic North Atlantic and North 1287  
Pacific. *Science* **293**, 847–849. 1288
- Zhu X. K., O’Nions R. K., Guo Y. and Reynolds B. C. (2000) 1289  
Secular Variation of Iron Isotopes in North Atlantic Deep 1290  
Water. *Science* **287**, 2000–2002. 1291

*Associate editor:* Timothy W. Lyons 1293

UNCORRECTED PROOF